ACS OMEGA

Open Access

http://pubs.acs.org/journal/acsodf

Article

Ion-Exchange Resin/Carrageenan-Copper-Based Nanocomposite: Artificial Neural Network, Advanced Thermodynamic Profiling, and Anticoagulant Studies

Sana Haider, Sami Ullah, Mohsin Kazi, Fouzia Qamar, Tariq Siddique, Rubia Anwer, Saeed Ahmad Khan, and Saad Salman*

Cite This: *ACS Omega* 2024, 9, 23873−23891

Read Online

ACCESS | Metrics & More | Article Recommendations

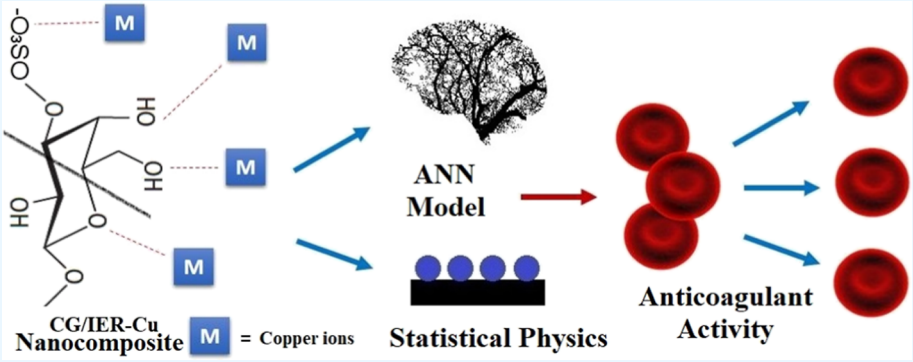

ABSTRACT: Carrageenan (CG) and ion exchange resins (IERs) are better metal chelators. Kappa (κ) CG and IERs were synthesized and subjected to copper ion (Cu^{2+}) adsorption to obtain DMSCH/κ-Cu, DC20H/κ-Cu, and IRP69H/κ-Cu nanocomposites (NCs). The NCs were studied using statistical physics formalism (SPF) at 315−375 K and a multilayer perceptron with five input nodes. The percentage of Cu^{2+} uptake efficiency was used as an outcome variable. Via the grand canonical ensemble, SPF gives models for both monolayer and multilayer sorption layers. For in vitro anticoagulant activity (ACA), the activated partial thromboplastin time were calculated using 100 μL of rabbit plasma incubated at 37 °C. After 2 min, 100 L of 0.025 M $CaCl_2$ was added, and the clotting time was recorded for each group (n = 6). The results demonstrated that the key covariables for the adsorption process were pH and concentration. The results of artificial neural network models were comparable with the experimental findings. The error rates varied between 4.3 and 1.0%. The prediction analysis results ranged from 43.6 to 89.2. The ΔG and ΔS values for IRP69H/κ-Cu obtained were −18.91 and −16.32 and 26.21 and 22.74 kJ/mol for the temperatures 315 and 345 K, respectively. Adsorbate species were perpendicular to the adsorbent surfaces, notwithstanding the apparent importance of macro- and micropore volumes. These adsorbents typically fluctuate with temperature changes and contain one or more layers of sorption. Negative and positive sorption energies correspond to endothermic and exothermic processes. The biosorption energy (E1 and E2) values in this experiment have a value of less than 23 kJ mol^{-1}. Complex SPF models' energy distributions validate surface properties and interactions with adsorbates. At a concentration of 100 μg/mL, DC20H/κ-Cu^{2+} exhibited an ACA of only 8 s. These NCs demonstrated better greater ACA with the order DC20H/κ < DMSCH/κ < IRP69H/κ. More research is needed to rule out the chemical processes behind the ACA of CG/IER-Cu NCs.

1. INTRODUCTION

The utilization of copper ions (Cu^{2+}) in medical practices spans centuries, supported by thorough documentation that attests to its enduring therapeutic efficacy.[1,2] Cu^{2+} can be administered for therapeutic benefits through diverse modalities, such as dietary supplementation, topical applications, and integration into medical devices, showcasing its versatility in healthcare interventions.[3] Cu^{2+} is frequently employed in dietary supplements to address or preempt Cu^{2+} deficiency, a state linked to issues like anemia, bone irregularities, and various health complications. Additionally, Cu^{2+} finds therapeutic application in topical forms, like Cu^{2+}-infused clothing and wound dressings, aimed at mitigating symptoms of

Received: February 28, 2024
Revised: April 21, 2024
Accepted: April 29, 2024
Published: May 20, 2024

arthritis and other inflammatory ailments. Furthermore, Cu^{2+}-impregnated wound dressings serve to thwart infections and foster the process of healing.[4]

Artificial intelligence (AI) models have been increasingly used in adsorption studies to predict adsorption properties, optimize adsorption conditions, and design new adsorbents. Artificial neural networks (ANNs) demonstrate the adsorption behavior by training the network on experimental data. ANNs can capture complex nonlinear relationships between input and output variables and predict adsorption performance with high accuracy, whereas support vector machines (SVMs) have been used in adsorption studies to predict adsorption capacity, selectivity, and kinetics.[5] SVMs have the advantage of being able to handle high-dimensional data and can make accurate predictions with relatively small data sets.[6] AI models have shown promising results in adsorption studies and have the potential to accelerate the development of new adsorbents and optimize adsorption processes.[7,8]

The molecular mechanisms of adsorption can also be predicted through a well-known mathematical model known as statistical physics formalism (SPF).[9] One of the key concepts in SPF is the partition function (PF), which describes the probability distribution of molecules in each system. The PF is used in adsorption research to determine a system's equilibrium adsorption parameters, including the heat of adsorption and isotherms. The molecular interactions between the adsorbate and adsorbent, the temperature, and the pressure affect the PF.[10]

Carrageenan (CG) is a naturally occurring polysaccharide that is derived from seaweed. While it has many applications in the food industry as a stabilizer and thickener, there are shreds of evidence to suggest that CG also has anticoagulant activity (ACA).[11,12] They are comprised of degraded and nondegraded forms such as kappa (κ-), lambda (λ-), iota (ι-), mu, nu, ksi, beta, and theta CG.[12,13] The chemical structure reveals that only ι- and κ- have 3,6-anhydro bridges, while these bridges are not seen in λ-.[14] It is believed that the presence or absence of these bridges and structural orientation gives ACA to CG.[15,16] The mechanism of ACA followed by CG is similar to other sulfated polysaccharides (SP).[16−18] Among other SP, heparin is a naturally occurring sulfated glucosaminoglycan composed of alternating uronic acid and α-D-glucosamine connected by α-(1 → 4) bonds. The serine proteinases involved in the blood clotting cycle are inhibited by heparin.[19] Only antithrombin (AT)-III interacts with heparin in the bloodstream. By inactivating thrombin, the heparin-AT-III complex also significantly increases the inhibitory action on other proteinases involved in blood clotting.[20] Their ACA typically diverges from heparin and entails contact with proteinases that are not heparin's targets[20] but produce comparable results.[21] The ACA of the partially oxidized κ-CG derivative was superior to that of the fully oxidized CG.[22,23] The functional group modification of CG by introducing carboxyl groups had a synergistic effect on the ACA.[23] These findings demonstrated that structural alterations to CG enhance or diminish its ACA. The chemical changes in CG are laborious and time-consuming and do not provide efficient ACA; therefore, a more economical surface modification is preferred.[24−26]

Divalent cations can participate in the competitive complexation of blood proteins.[27] C reactive protein (CRP) levels were favorably correlated with Cu^{2+} plasma concentrations. This suggested that a higher Cu^{2+} concentration may strengthen an elevated CRP level. Previous research has emphasized a strong connection between CRP and levels of Cu^{2+}. The interaction between heparin, fibrinogen, and Cu^{2+} can indeed have significant effects on fibrinogen's sedimentation coefficient. Heparin is a well-known anticoagulant that functions by enhancing the activity of antithrombin-III, a natural inhibitor of thrombin and other coagulation factors. Heparin also interacts with fibrinogen, influencing its polymerization into fibrin strands, which are essential for blood clot formation.[28] The doped Cu^{2+}-nickel manganite composite hindered platelet aggregation and interfered with the blood coagulation cascade.[29] Cu^{2+} has been found to inhibit several key factors involved in the coagulation process, including thrombin and factor Xa, which are crucial for the conversion of fibrinogen to fibrin, the main component of blood clots. Cu^{2+} can interfere with platelet activation and aggregation, further inhibiting clot formation. However, it is essential to conduct thorough biocompatibility and toxicity studies to ensure the safety and efficacy of copper ion-impregnated/loaded nanocomposites for biomedical applications. Cu^{2+} complexes are reported to treat thrombosis since they inhibit polyphosphate activity.[30] The in vitro ACA of Cu^{2+} sulfate reduced the thrombin time and suppressed the platelet aggregation. Preincubating Cu^{2+} sulfate with fibrinogen slightly reduced its capacity to clot.[31] Further research is needed to optimize the design and fabrication of engineered materials that can impregnate Cu^{2+} to enhance their anticoagulant properties while minimizing any potential adverse effects.

Ion-exchange resins [ion exchange resin (IER)] have been studied for their ability to bind to certain metals but do not have intrinsic ACA. The mechanism by which IER binds to biomolecules in the blood is based on the ion exchange principle. These resins have charged groups that attract and bind to ions of the opposite charge. The purpose of IER was to chelate Cu^{2+}, which will elicit ACA activity. Various studies utilized diverse strategies for the removal of Cu^{2+} from aqueous solutions. It encapsulates a multitude of studies investigating various adsorbents and modification techniques aimed at enhancing Cu^{2+} removal efficiency. These studies encompass a wide spectrum of factors including the concentration of Cu^{2+}, duration of contact, dosage of adsorbents, and modification methods applied. From H_2SO_4 impregnation[32] to steam activation, phosphoric acid treatment to AgNPs impregnation, an array of modification techniques have been explored to augment adsorption capacity. A diverse range of natural materials as adsorbents, including hazelnut shells,[32] hulls of *Ceiba pentandra*,[33] *Typha latifolia* L.,[34] pomelo peels,[35] green vegetable waste,[36] pistachio shells, apricot stone, almond, walnut,[37] grape bagasse,[38] hazelnut husk,[39] lignocellulose,[9] pecan shells,[40] rubber wood sawdust,[41] pinewood sawdust,[42] peanut shells,[43] apricot stone,[44] chestnut shells, and grape seeds[45] were previously utilized. The reported uptake percentages and capacities vary across these studies, with some adsorbents demonstrating high efficiency (>80%) while others exhibit moderate to substantial capacities. These findings underscore the importance of exploring novel adsorbents and modification techniques for the effective removal of heavy metal ions[46−51] from aqueous environments and highlight the potential of utilizing diverse natural materials for environmental remediation purposes.

Herein, we utilized advanced AI models for the biosorption of Cu^{2+} using IER/CG blends by applying multilayer perceptrons (MLP). MLP, an ANN, is utilized to model nonlinear interactions between input variables such as

https://doi.org/10.1021/acsomega.4c01540
ACS Omega 2024, 9, 23873−23891

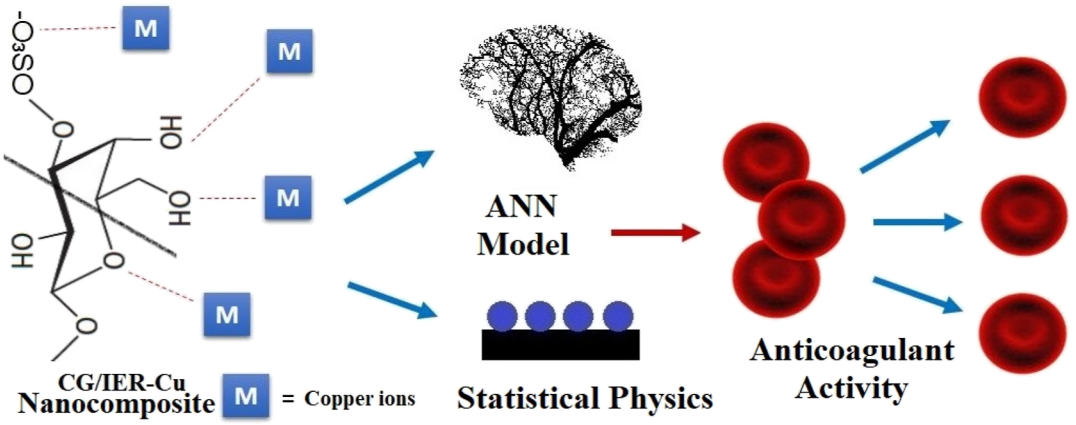

Figure 1. SPF and ANN modeling of CG/IER-Cu NC and their ACA.

temperature, pH, dose, output variable, and the percentage of Cu^{2+} uptake. Another aspect of the study involved the use of a SPF model to interpret the steric and energetic aspects of Cu^{2+} biosorption, combining both the size and shape of binding sites and adsorption strength. Reagents include κ-, λ-, and ι- CG as carriers, $CuSO_4$ as a source of Cu^{2+}, and HCl and NaOH for pH adjustment. Surface modification of DMSCH/κ-, DC20H/κ-, and IRP69H/κ- is carried out through Cu^{2+} adsorption, and the ACA was studied in vitro using rabbit plasma. Statistical analysis was performed using one-way ANOVA and the Tukey test. Figure 1 illustrates the main theme of the study.

2. MATERIALS AND METHODS

IER/CG blends were used to study the biosorption of Cu^{2+} using MLP. It is a popular sort of ANN employed in many domains, including adsorption research. Modeling intricate nonlinear interactions between input and output variables is where MLP has a practical utility. MLP can be used in adsorption studies to forecast a material's capacity for adsorption depending on a variety of input factors, including temperature, pH, dose, surface area, and adsorbate concentration. By forecasting the ideal operating parameters for maximum adsorption capacity, MLP may also be utilized to improve the adsorption process. To collect the data, five covariables (input nodes) were employed in the input layer. As an outcome variable, the percentage of uptake of Cu^{2+} ions was taken. A variety of nodes were utilized to identify the ideal number of veiled nodes. The brief method of biosorption studies is reported elsewhere.[8,9]

2.1. SPF Model Development for Energetic and Steric Interpretation. SPF is a theoretical approach that can be used to model the behavior of complex systems, including adsorption processes. The initial dose at a constant pH of 5 was 0.5 g in 50 mL of solution at 315, 345, and 375 K to investigate the steric and energetic interpretation of Cu^{2+} biosorption. SPF can be used to develop a model that provides a deep insight into the molecular phenomenon involved in the biosorption process.[10] The steric interpretation of Cu^{2+} biosorption can be described using a hard-sphere model, which assumes that the Cu^{2+} and the binding sites on the biomass are hard spheres that cannot overlap.[52] To combine the steric and energetic interpretations of Cu^{2+} biosorption, the SPF model can be developed that takes into account both the size and shape of the binding sites and the strength of the adsorption interaction. This model can be used to predict the adsorption capacity of the biomass as a function of the Cu^{2+} concentration, temperature, and other relevant parameters. The SPF model can provide a complete understanding of the adsorption process and help to optimize the conditions for maximum biosorption efficiency.[53]

2.1.1. Reagents and Chemicals. κ-, λ-, and ι- CG (Sigma-Aldrich, USA) were selected as carriers for the metal-ion adsorption. $CuSO_4$ (Saarchem, SA) was used as a source of Cu^{2+}. HCl and NaOH (BDH Chemicals, Kuwait) were employed for the adjustment of pH, and as a solvent, the ultrapure water (18.2 mΩ cm, 25 °C) was used. For anticoagulation studies, trisodium-citrate (Sigma-Aldrich, USA), a free-calcium binder, heparin (Sigma-Aldrich, USA), and thrombin (Sigma-Aldrich, USA) were utilized.

2.1.2. Surface Modification of DMSCH/κ-, DC20H/κ-, and IRP69H/κ- through Cu^{2+} Adsorption. For metal adsorption, $CuSO_4$ (Saarchem, SA) was used. HCl and NaOH (BDH Chemicals, Kuwait) were used for pH adjustment. A precisely weighed amount of 0.1, 0.2, and 0.5 g of each CG/IER were mixed with 10, 30, and 60 mL of metal ions solutions ($CuSO_4$) in 100 mL conical flasks for the determination of the adsorption of metal ions over the CG and CG/IER. The formed metal coordinated complexes were shaken at 25 °C on an end-to-end shaker (DAIHAN WSB-30, USA) for 24 h. The filtrates were then subjected to further analysis at different values of pH ranging from 1 to 9. The spectrophotometric analysis of the conc. of metal ions with CG/IER in the aqueous phase was carried out through Optima, SP-300 spectrophotometer (Tokyo, Japan) at 550 nm for Cu^{2+}, respectively, at different time intervals of 20−380 min. The detailed methods of isotherm, kinetic models, and their equations are reported elsewhere.[8,54] All the experiments were conducted in triplicates.

2.1.3. ACA. In our in vitro study of ACA, we employed the HemosIL kit (Instrumentation Laboratory Company, Bedford, MA, USA) in conjunction with the KL-340 coagulation analyzer (Meizhou Cornley, Hi-Tech Company, Ltd.) to measure activated partial thromboplastin times activated partial thromboplastin time (aPTT). The experimental procedure involved incubating 100 μL of rabbit plasma at 37 °C with 100 mL of heparin, polysaccharide, or saline samples. One minute after aPTT, 100 μL of reagent was added, followed by the addition of 100 L of 0.025 M $CaCl_2$ after 2 min. The clotting time was then recorded for each group (n = 6). It is important to note that this study involving animals received ethical approval from the Ethical Committee of the University of Lahore, Islamabad Campus. All protocols related to animal

https://doi.org/10.1021/acsomega.4c01540
ACS Omega 2024, 9, 23873−23891

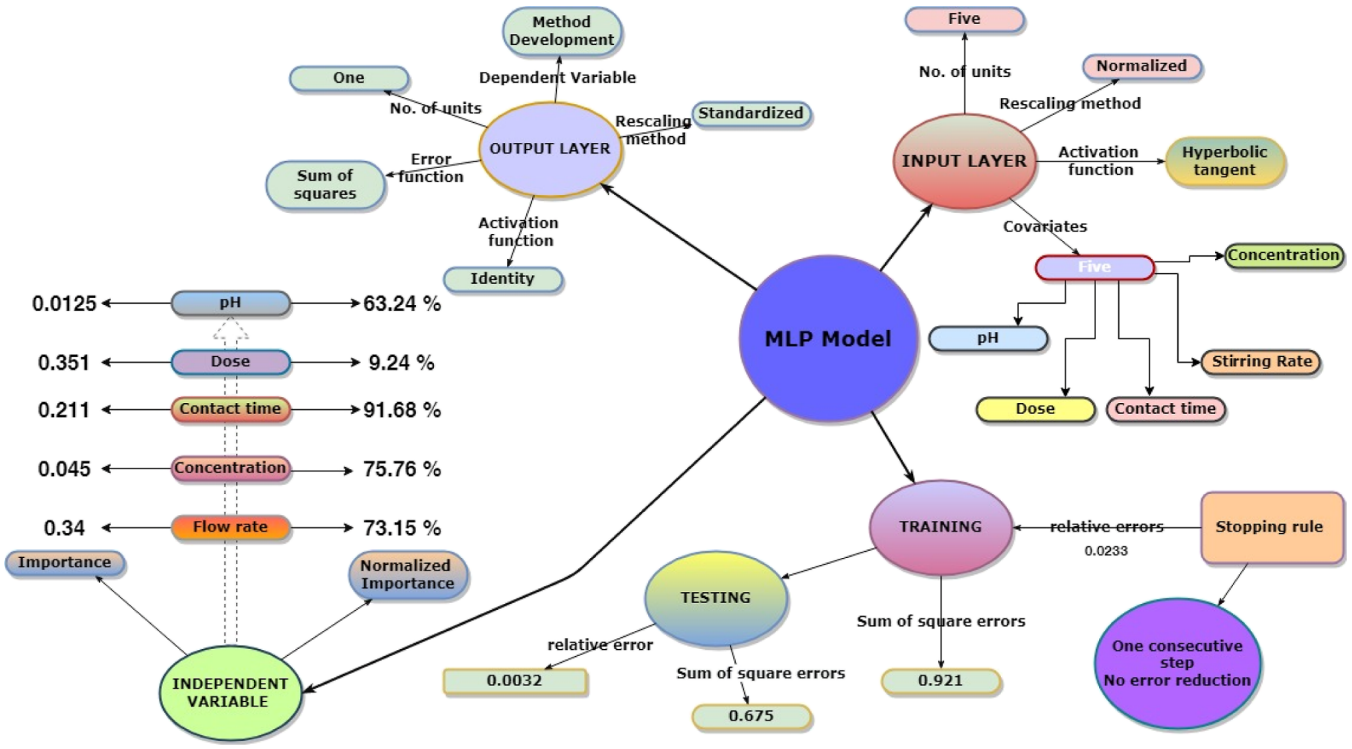

Figure 2. ANN modeling training variables, basic structure, and results of IER/CG- Cu NC.

care were meticulously followed to ensure the well-being and ethical treatment of the animals throughout the experimentation.

2.1.4. Statistical Analysis. To assess the statistical significance of our observations, the data from the samples were subjected to one-way and two-way ANOVA. This statistical test was used to compare the means of three or more groups to determine whether there are statistically significant differences between them. In this context, it suggests that multiple groups of data were compared, likely corresponding to different experimental conditions or treatments. A significance level of probability (p-value) of less than 0.05 was chosen for determining statistical differences. In other words, if the probability of observing the differences between groups by chance alone was less than 5%, then those differences were deemed significant. Software such as GraphPad Prism and SPSS 25.0 were utilized for the analysis of anticoagulant studies.

For ANN and SPF, we utilized Python 3.11.8 and Mathematica 11. Python is a versatile programming language commonly used in scientific computing and data analysis. We utilized libraries such as NumPy, SciPy, and SymPy to provide functionalities for statistical physics calculations, simulations, and data analysis. Mathematica is a computational software system that offers extensive capabilities for symbolic and numerical calculations. It includes built-in functions for solving statistical physics problems, performing simulations, and visualizing results.

3. RESULTS AND DISCUSSION

3.1. Artificial Neural Network. AI models can be used for predicting metal adsorption in various materials. AI models can provide a fast and accurate way to predict metal adsorption in various materials, which can help researchers develop new materials with improved adsorption properties.

For Cu^{2+} biosorption on KC/IER, an ANN model was applied. Figure 2 depicts the network information, case processing summaries, independent variable significance, and model summaries. The independent variable was divided into two categories: (a) importance and (b) normalized importance. Training and testing were included in model summaries. The network information is made up of two layers: input and output. Figure 2 shows the variables/covariates and their values. The maximum iteration was 100, while the learning rate and momentum faction were both 0.8. QuickProp was used as the learning algorithm, using Tanh as the transfer function.

The connection type was multilayer normal feed forward, with only one concealed layer. The proposed mechanism of adsorption is given in Figure 3.

The MLP model 6-3-1 was utilized to investigate the five covariables of absorption of Cu^{2+}; the input, output, and buried layers were included. The MLP model 6-3-1 was used for training with no data from 100 runs being excluded. A continuous simulation approach was used to create a link between weight and bias throughout the training phase. Nonetheless, the results revealed little difference between predicted and normalized values. In biosorption investigations, the effective covariables were found to be dosage, pH, and concentration. The results showed that ANN modeling might be very effective in predicting biosorption investigations. The ANN models agreed with the experimental results. Nonetheless, as seen in 3C and 3D, there were minor variations in the results. The other reported NCs used for the Cu^{2+} uptake have been provided in Table 1.

3.1.1. Table Description. The concentration of Cu^{2+} (mg/L) indicated the initial concentration of Cu^{2+} in different solutions used in various experiments. It ranged from 1.5 to 1000 mg/L in different studies; time of contact (min) specifies the duration of time for which the adsorbent material was in contact with the solution containing Cu^{2+}. The time ranges

https://doi.org/10.1021/acsomega.4c01540
ACS Omega 2024, 9, 23873−23891

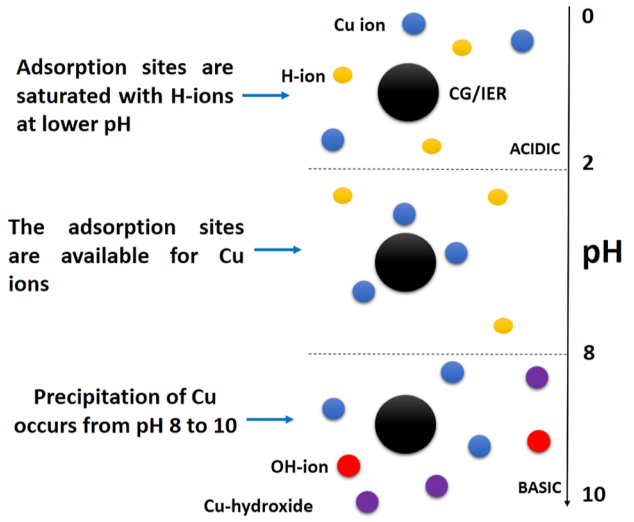

Figure 3. Mechanism of Cu^{2+} adsorption over the surface of the composite.

from 1440 min (24 h) to 4320 min (72 h) in different experiments; dosage (g/L) refers to the amount of adsorbent material used per unit volume of solution. The dosage varied from 0.05 to 25 g/L; modification included impregnation with acids (e.g., H_2SO_4 and H_3PO_4), steam activation, or the use of specific chemicals (e.g., KOH and $ZnCl_2$); the uptake percentage ranged from >80 to >90% in most cases; isotherm indicates the type of adsorption isotherm used to model the adsorption process. The Langmuir-type isotherm (LAI) is commonly mentioned as the pH of the solution during the adsorption process. pH values range from 2 to 7; uptake capacity (mg/g) is the amount of Cu^{2+} adsorbed per unit mass of the adsorbent material. Values range from 5.72 to 229 mg/g; kinetic models describe the adsorption kinetics, such as pseudo-second-order (PSO); adsorbents are various agricultural waste products like hazelnut shells, grape bagasse, pecan shells, etc. Predicted Percentage of Uptake of Cu^{2+} ions.

These are the predicted values of the percentage of uptake of Cu^{2+} for each sample based on the input features (covariables) provided in the data set. The values range from approximately 43 to 89%. Higher values indicate a higher predicted uptake percentage, while lower values indicate a lower predicted uptake percentage. The predicted uptake percentages provide insights into the effectiveness of different adsorbents and conditions in the adsorption process. Adsorbents and conditions associated with higher predicted uptake percentages may be considered more effective in removing Cu^{2+} from the solution.

Conversely, adsorbents and conditions associated with lower predicted uptake percentages may be less effective or may require optimization to enhance their performance in the adsorption process. These predictions can guide further experimentation and optimization efforts in adsorption research to improve the efficiency of Cu^{2+} removal using various adsorbents and conditions.

3.2. Results of SPF. The first layer of adsorbate molecules forms a monolayer on the surface, with the molecules oriented in a specific direction to optimize their interaction with the surface. Once the first layer is formed, the adsorbate molecules continue to be adsorbed onto the surface, forming additional layers of molecules on top of the first layer.[53] The SMM and model with single energy (MSE) values were plotted using GraphPad Prism 9.4.1. A 20−30% drop was seen when the temperature was raised to 315−375 K. Heat weakens the bond between Cu^{2+} and the sorbent surface, making it feasible. Adsorption capacity, which seems to be closely related to micropore volume, appears to be governed mostly by functional group interactions. The disadvantage of the double-layer model with two energies is that it produces lower coefficients of determination. SMM was used to explore the properties of IER-CG. It was utilized to look at the biosorption mechanisms that occur during Cu^{2+} absorption. The double-layer model is a theoretical model used to describe the electrostatic interactions between charged surfaces and ions in solution. The SPF for the double-layer model involves considering the system as a collection of particles in thermal equilibrium with their environment. The energy associated with the system is given by the Hamiltonian, which includes terms for the surface energy (Table 2).

The number of Cu^{2+} ions captured on a single binding site of an adsorbent can be analyzed using SPF. In this context, the binding site is a location on the surface of the adsorbent where a Cu^{2+} ion can bind through noncovalent interactions. The SPF for analyzing the number of Cu^{2+} ions captured on a single binding site involves considering the system as a collection of particles in thermal equilibrium with their environment. The energy associated with the system is given by the Hamiltonian, which describes the energy of the system as a function of the positions and momenta of the particles.[10,55]

The number of Cu^{2+} ions captured on a single binding site of an adsorbent can be analyzed using SPF by considering the system as a collection of particles in thermal equilibrium with their environment. The probability distribution of the number of Cu^{2+} captured on the binding site can be expressed as a function of the binding energy and the chemical potential of the Cu^{2+} in the surrounding environment and can be calculated using techniques such as Monte Carlo simulations or molecular dynamics simulations.[56−58] Our modeling suggests that a single binding site can interact with many Cu^{2+} ions. The highest value of n_{ms} for IER-CG discovered at 375 K is 1.54 (Figure 4). According to this, around one-third of the Cu^{2+} has a single dock and two-thirds has a double dock. Ionic aggregation appears to be directly influenced by temperature 10. The thermodynamic attributes are provided in Table 2.

3.2.1. SPF Model.

$$z_{gc} = \sum_{N_s} e^{-\beta(-\varepsilon_i-\mu)N_s} = 1 + e^{\beta(\varepsilon_1+\mu)} + e^{\beta(\varepsilon_1+\varepsilon_2+2\mu)}\frac{1 - e^{\beta(\varepsilon_2+\mu)^{N_L}}}{1 - e^{\beta(\varepsilon_2+\mu)}} \quad (1)$$

the equation described the PF—z_{gc} for a system involving Cu^{2+} adsorption on a NC. The simplified form of this equation is the PF in statistical mechanics (SM), often used to describe the statistical properties of a system of particles or molecules.

The terms are explained regarding Cu^{2+} adsorption on a NC in the following: z_{gc} is the PF, which is a fundamental concept in SM. It represents the sum of the exponential terms involving different states of Cu^{2+} adsorption on the NC. $\sum N_s$ indicates a summation of the various possible states of Cu^{2+} adsorption on the NC. In other words, it considers all the possible configurations of Cu^{2+} on NC. $e^{\beta(\varepsilon_1+\mu)}$ describes the probability of finding the system in a specific state N_s. Where each variable represents: β is expressed as 1/kBT and is related to the

https://doi.org/10.1021/acsomega.4c01540
ACS Omega 2024, 9, 23873−23891

Table 1. Biosorption of Cu^{2+} Over CG/IER-Cu NCs[a]

study	conc. Of Cu^{2+} (mg/L)	time of contact (min)	dosage (g/L)	modification	uptake (%)	isotherm	pH	uptake capacity (mg/g)	kinetic models	adsorbent	predicted vs experimental % of Cu^{2+} uptake	study description
32	25−200	90	0.5−3	H_2SO_4 impregnation		LAI	2−6	58.27	PSO	hazelnut shells	77.57	the hazelnut shells were modified using H_2SO_4 impregnation. While the uptake percentage and uptake capacity are not provided, the adsorbent showed good potential for Cu^{2+} removal
33	80	90	0.1−2	steam activation		LAI	6	20.8	PSO	hulls of Ceiba pentandra	43.66	the hulls were subjected to steam activation. Although specific uptake values are not provided, the adsorbent showed a moderate uptake capacity of 20.8 mg/g
34	40−200 mol/L	120	2	H_3PO_4	89.36	LAI	6	34.48	PSO	Typha latifolia L	83.57	Typha latifolia L. was treated with H_3PO_4. It exhibited a high uptake percentage of 89.36% and a corresponding uptake capacity of 34.48 mg/g, indicating efficient Cu^{2+} removal
35	100−300	300	0.05	K_2CO_3		LAI	6	139.08	PSO	pomelo peels	68.13	the adsorbent, prepared from pomelo peels and modified with K_2CO_3, displayed a high uptake capacity of 139.08 mg/g, indicating excellent Cu^{2+} adsorption efficiency
36	1.5	120	0.6	KOH	76.36	LAI	3.5	75	PSO	green vegetable waste	73.75	treated with KOH, green vegetable waste showed a substantial uptake percentage of 76.36% and a corresponding uptake capacity of 75 mg/g, suggesting efficient Cu^{2+} removal
37	30		0.1−1		>90		6−10		PSO	pistachio	87.11	specific experimental details are not provided, but the adsorbent exhibited a high uptake percentage (>90%), indicating excellent Cu^{2+} adsorption potential
37					>80		6−10		PSO	hazelnut, apricot stone, almond, Walnut	87.11	while specific experimental details are lacking, the composite adsorbent showed a high uptake percentage (>80%), suggesting efficient Cu^{2+} removal potential
38	100	300	5	H_3PO_4		LAI and DRI	6	43.47	PSO	grape bagasse	79.03	treated with H_3PO_4, grape bagasse exhibited a moderate uptake capacity of 43.47 mg/g, indicating moderate Cu^{2+} adsorption efficiency
39	5−200	60	2−20	$ZnCl_2$		LAI and FAI	6.7−7	6.645	PSO	hazelnut husk	59.39	the hazelnut husk was treated with $ZnCl_2$. The uptake capacity was found to be 6.645 mg/g, indicating moderate adsorption efficiency
9	50−1000	180	3.39	AgNP impregnation		LAI	2−7	229	PSO	lignocellulose of XS/FT	83.87	the adsorbent, modified with AgNPs impregnation displayed a high uptake capacity of 229 mg/g, indicating excellent Cu^{2+} adsorption efficiency
40	10−500	4320	1	phosphoric acid		LAI	3.6	95	PSO	pecan shells	89.22	treated with phosphoric acid, pecan shells exhibited a substantial uptake capacity of 95 mg/g, suggesting efficient Cu^{2+} removal potential
41	10−40	240	5	H_2SO_4		LAI	6	5.72	PSO	rubber wood sawdust	49.46	the adsorbent, treated with H_2SO_4, showed a lower uptake capacity of 5.72 mg/g, indicating relatively lower Cu^{2+} adsorption efficiency
42	25−200	60	2	H_3PO_4			6.2	20.2	PSO	pinewood sawdust	47.61	the adsorbent, treated with H_3PO_4, exhibited a moderate uptake capacity of 20.2 mg/g, indicating moderate Cu^{2+} adsorption efficiency
43	20 mM	1440	10				4.8	50.39	PSO	peanut shells	84.36	while specific experimental details are not provided, peanut shells showed a moderate uptake capacity of 50.39 mg/g, indicating moderate Cu^{2+} adsorption efficiency
44		1880	2	H_2SO_4	97.48		6	24.21	PSO	apricot stone	86.22	treated with H_2SO_4, apricot stone exhibited a high uptake percentage of 97.48% and a corresponding uptake capacity of 24.21 mg/g, indicating efficient Cu^{2+} removal
45	25−1000	90	25	$ZnCl_2$ impregnation		FAI	5	100	PSO	chestnut shell	87.11	both adsorbents, modified with $ZnCl_2$ impregnation, exhibited moderate uptake capacities of 100 mg/g and 48.78 mg/g, respectively, indicating moderate Cu^{2+} adsorption efficiencies
45	25−1000	120	25	$ZnCl_2$ impregnation		FAI	5	48.78	PSO	grape seed	62.20	

[a]LAI—Langmuir biosorption isotherm; DAI—Dubinin−Radushkevich isotherm; FAI—Freundlich adsorption isotherm; PSO—Pseudo-second order.

https://doi.org/10.1021/acsomega.4c01540
ACS Omega 2024, 9, 23873−23891

Table 2. Thermodynamics Profiling of CG/IER-Cu^{2+} (Theoretical and Practical Attributes)[b]

compound	log β_{abc} [a]	equilibrium constants			ΔG (kJ/mol)			ΔS (kJ/mol)			ΔH (kJ/mol)	G (H/P)	$\Delta_r G$ (H/P)
		315.15[a]	345.15	375.15	315.15	345.15	375.15	315.15	345.15	375.15			
IRP69/kappa-Cu	3.28 ± 0.02	3.61	3.001	2.87	−18.91	−17.31	−16.32	26.21	24.32	22.74	−9.01	−1391.185485	−0.196359
kappa		3.12	2.91	2.61	−16.78	−15.63	−14.39	25.43	23.46	22.77	−9.39	−325.066751	
IRP69H		2.18	1.54	1.14	−16.13	−15.48	−14.11	18.38	16.66	14.45	−8.22	−1391.185485	

[a]At pH range 2−11. [b]All temperature values are in Kelvin. (H/P) − (Hartree/particle), 1 hartree/particle = 2.6255048 × 10^3 kJ/mol. logβabc1 represents the logarithm of some equilibrium constant (βabc1). Equilibrium constants typically represent the ratio of products to reactants at equilibrium in a chemical reaction. Equilibrium constants are values related to the equilibrium constants of the compounds at different temperatures. ΔG (kJ/mol) represents the change in Gibbs free energy for the reactions involving the compounds, measured in kilojoules per mole (kJ/mol). ΔS (kJ/mol) represents the change in entropy for the reactions, also measured in kilojoules per mole (kJ/mol). ΔH (kJ/mol) represents the change in enthalpy for the reactions, measured in kilojoules per mole (kJ/mol). G (H/P) is the ratio involving Gibbs free energy and Hartree per particle. $\Delta_r G$ (H/P) represents the change in Gibbs free energy per Hartree per particle. The pH range for the experiments is 2−11, and all temperature values are given in Kelvin.

system's thermal energy. ε are the binding energies. ε_1 and ε_2 represent the binding energies of Cu^{2+} to the NC. The energy required to add/remove the particle from the system, μ is the chemical potential has been widely used. N_s is the number of Cu^{2+} in the system.

The equation is a sum of different states, with each state's contribution being determined by the Boltzmann factor, which depends on the energy (binding energy and chemical potential) and the number of particles in that state. The last part of the equation involves a fraction that represents the grand-canonical partition-function (GCPF). It accounts for the normalization of the probabilities. This equation is used to calculate the PF for a system where Cu^{2+} is absorbed into a NC. The different energy states, the chemical potential, and temperature are all considered to determine the overall statistical properties of the system. The PF is a key concept in SM, and it is often used to derive various thermodynamic properties of the system, such as the free energy, entropy, and average occupancy of particles. To account for a more complex system involving multiple replicas or subregions of the NC, eq 1 can be derived to obtain

$$Z_{gc} = \left[1 + e^{\beta(\varepsilon_1+\mu)} + e^{\beta(\varepsilon_1+\varepsilon_2+2\mu)}\frac{1 - e^{\beta(\varepsilon_2+\mu)N_L}}{1 - e^{\beta(\varepsilon_2+\mu)}}\right]^{D_{sr}} \quad (2)$$

This equation is a modified form of the PF in SM, tailored to describe the adsorption of Cu^{2+} on a NC. The modified equation is an extension of the original equation and includes an additional exponent (D_{sr}) at the end:

In this equation, D_{sr} appears to be an exponent that accounts for the number of replicas or subregions (s) of the NC. This modified equation described the overall PF for a system of Cu^{2+} adsorption on an NC with multiple subregions or replicas.

This equation depends on the system and the physical model being used. However, it is likely that the derived equation accounts for the fact that there are multiple subregions (replicas) of the NC where Cu^{2+} adsorption can occur. Each subregion may have slightly different properties, such as the number of binding sites, energies, or chemical potentials. To derive this equation, eq 1 for a single NC was extended to consider the contributions from multiple subregions. The exponent D_{sr} is introduced to represent the multiplication of PFs for each subregion, effectively combining their statistical properties. This equation can be written as[59]

$$N_O = k_B T\frac{\partial \ln Z_{gc}}{\partial \mu} = D_{sr}k_B T\frac{\partial \ln z_{gc}}{\partial \mu} \quad (3)$$

here, N_0 represents the site occupation number, which is the average number of Cu^{2+} ions occupying the adsorbent receptor sites (R) on the NC. The equation tells us that N_0 depends on the derivative of the natural logarithm of the GCPF (Z_{gc}) concerning the chemical potential (μ). This equation is used to determine the average occupancy of the binding sites in the NC. D_{sr} represents the number of receptor sites (binding sites) within the NC. This equation is tailored to the NC scenario where multiple binding sites exist.

This equation is important in understanding the adsorption of Cu^{2+} onto a NC material. Site occupation number, N_0, is a measure of how many Cu^{2+}, on average, are bound to the receptor sites (binding sites) on the NC. It is related to the chemical potential (μ), temperature (T), and the properties of

https://doi.org/10.1021/acsomega.4c01540
ACS Omega 2024, 9, 23873−23891

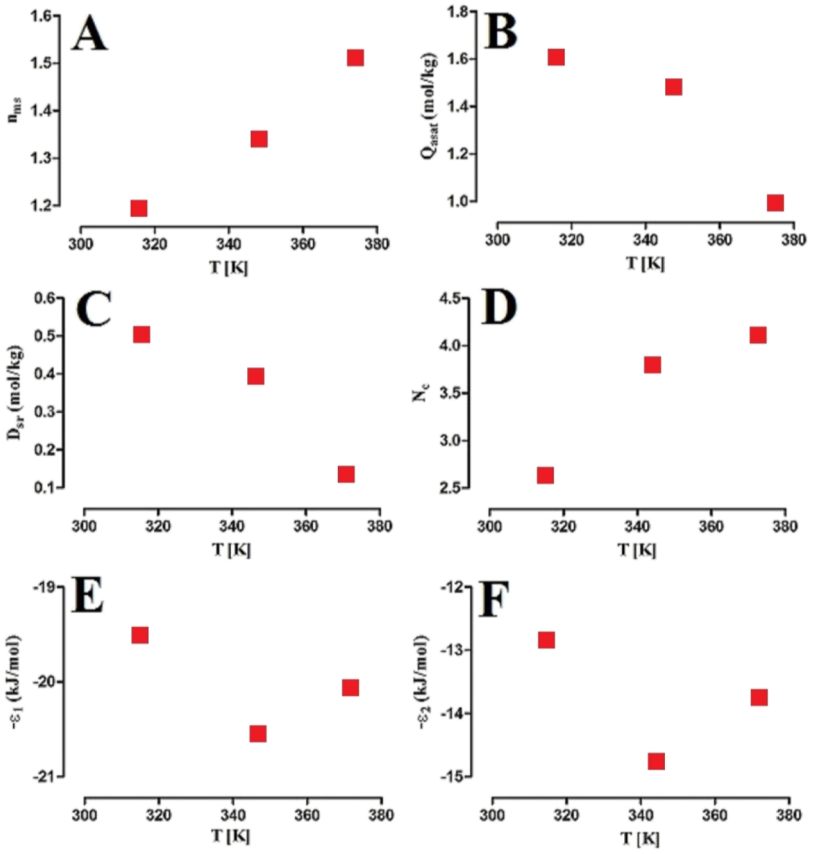

Figure 4. Model description of SMM for (A) Cu^{2+} biosorption over NCs through the number of captured species, (B) saturation capacity of Cu^{2+} over NCs, (C) NCs' receptor site density, and (D) sum of formed layers over NCs (E,F) Cu^{2+} biosorption energies from at 1 bar pressure with a temperature range of 315−375 K.

the binding sites within the NC. In GCPF, Z_{gc} is a mathematical construct that describes the statistical behavior of a system in equilibrium with a reservoir at a given chemical potential. In this case, it represents the behavior of Cu^{2+} interacting with binding sites on the NC.

The equation for N_o can be derived from the grand canonical ensemble theory in SM. It is based on the concept that the average number of particles in a system can be related to the derivative of the logarithm of the PF concerning the chemical potential. Considering the Cu^{2+} adsorption on a NC, this equation is derived by considering the statistical behavior of ions interacting with binding sites. It relates the average number of ions bound to the site to the properties of the NC and the thermodynamic variables.

This equation is useful for understanding the adsorption of Cu^{2+} on NC. It helps quantify how many Cu^{2+} are likely to bind to the receptor sites on the NC at a given chemical potential and temperature. It is a fundamental concept in the study of adsorption processes and provides a way to connect the statistical behavior of particles with the thermodynamic properties of the system. By analyzing N_0 as a function of μ and T, researchers can gain insights into the adsorption behavior, predict how many Cu^{2+} ions will bind to the NC under different conditions, and optimize the material's performance for adsorption applications.

n_{ms} Cu^{2+} represents n_{ms} moles or entities of Cu^{2+} that are involved in the reaction. It shows the reactant side of the equation, indicating the Cu^{2+} before they bind to the receptor sites. "R" represents the adsorbent receptor sites. These are the sites or locations on a material or surface that can bind or adsorb Cu^{2+}. This is an equilibrium reaction, indicating that the binding of Cu^{2+} to receptor sites can occur in both directions. Cu^{2+} can bind to the receptor sites, and the bound Cu^{2+} can potentially dissociate from the sites, establishing an equilibrium. This equation describes a chemical equilibrium between Cu^{2+} and adsorbent receptor sites on a material or surface. It highlights that the process of Cu^{2+} binding to receptor sites involves a stoichiometric ratio, n_{ms}, which represents how many Cu^{2+} are required to bind to "n_{ms}" receptor sites. The equation is important in the context of adsorption processes, such as in environmental remediation or material science. It provides a fundamental understanding of how Cu^{2+} interacts with adsorbent surfaces and the equilibrium between the unbound and bound states. Researchers use this information to design and optimize materials for adsorption applications or to study the removal of Cu^{2+} from solutions. The value of n_{ms} would depend on the nature of the adsorbent and the properties of the Cu^{2+}.

When Cu^{2+} interacts with an adsorbent receptor site on a material or surface, the process typically involves a stoichiometric coefficient represented as n_{ms}. This coefficient describes the ratio of Cu^{2+} to adsorbent receptor sites involved in the binding process. The n_{ms} value indicates how many Cu^{2+} are required to bind to several receptor sites, and it is an important factor in understanding the reaction's stoichiometry. The equation is a representation of the chemical reaction that occurs when Cu^{2+} binds to adsorbent receptor sites. The equation can be written as

https://doi.org/10.1021/acsomega.4c01540
ACS Omega 2024, 9, 23873−23891

$$n_{ms}Cu^{2+} + R \rightleftarrows (Cu^{2+})_{n_{ms}}R \quad (4)$$

In the chemical system involving Cu^{2+} and binding sites, the chemical potential of Cu^{2+} is denoted as μm, which represents the energy or potential associated with the presence of these ions in the system. The number of Cu^{2+} captured or bound per binding site is indicated by n_{ms}, signifying the extent to which these ions interact with the available binding sites.

To describe the chemical potential at equilibrium in this system, we can use the concept of equilibrium in thermodynamics. At equilibrium, there is no net change in the system, meaning the system has reached a state of balance. In the case of Cu^{2+} and their binding sites, at equilibrium, the μm of Cu^{2+} will remain constant. This means that the energy or potential associated with the presence of Cu^{2+} will not change over time when the system is in equilibrium.

The relationship between the μm and the number of ions bound per binding site (n_{ms}) can be expressed mathematically to show that at equilibrium, there is a balance between the tendency of Cu^{2+} to interact with binding sites and any opposing factors that might cause them to unbind or leave the binding sites.

$$\mu_m = \mu/n_{ms} \quad (5)$$

The equation relates to the chemical potential (μm) of Cu^{2+} in a system where these ions are bound to some binding sites, and it expresses the chemical potential at equilibrium. The μm represents the chemical potential of Cu^{2+}. Chemical potential is a concept in thermodynamics that measures the energy of a particle in a system. In the context of ions or molecules, it represents the energy per unit quantity (in this case, per unit of Cu^{2+}). n_{ms} represents the number of Cu^{2+} bound to each binding site. This is essentially the stoichiometry of Cu^{2+} binding to these sites. For example, if each binding site can accommodate two Cu^{2+}, n_{ms} would be 2. This equation states that the chemical potential of Cu^{2+} (μ_m) at equilibrium is equal to the chemical potential of the entire system (μ) divided by the number of Cu^{2+} bound per binding site (n_{ms}).

At equilibrium, the chemical potential of the Cu^{2+} must be the same as the chemical potential of the system they are in. In other words, the chemical potential of the ions should be balanced with the rest of the system to reach a stable state. This equation helps express that relationship. It is worth noting that chemical potential is related to the free energy of a system, and this equation reflects the thermodynamic principles governing systems with ion binding. The chemical potential at equilibrium ensures that there is no net tendency for Cu^{2+} to move in or out of the binding sites, as their chemical potential is balanced with the surrounding environment.

The following equation relates to the chemical potential (μ_m) in the context of ideal gas translation PFs and is expressed using an approximation[60]

$$\mu_m = k_B T \ln \frac{N}{Z_{gtr}} \quad (6)$$

The eq 5 takes the form as (Khalfaoui et al., 2002)[61]

$$Z_{gtr} = V\left(\frac{2\pi m k_B T}{h^2}\right)^{3/2} \quad (7)$$

In this equation, the adsorbed molecule mass was denoted by m, whereas V is the gas volume and h is Planck's constant. In an ideal gas approximation, the translational PF can be calculated relatively easily. This approximation assumes that the gas particles are noninteracting, and their behavior can be described as if they were ideal, noninteracting particles. In such a case, the translation PF simplifies to a form that depends on the temperature and the mass of the gas particles. This equation is commonly used in SM to relate the chemical potential to the properties of an ideal gas system, making it a useful tool for understanding the behavior of particles in such systems.

The saturated vapor pressure (P_{vs}), vaporization energy (ΔE^v), and per unit volume of translation PF (Z_{gtr}) for an ideal gas can be expressed as[58]

$$Z_{gtr} = \beta P_{vs} e^{\Delta E^v/RT} \quad (8)$$

$$P_{vs} = \left(\frac{(2\pi m k_B T)^{3/2}}{h^3}\right)(k_B T)e^{-\Delta E^v/RT} \quad (9)$$

To determine the quantity of sorbed molecules on a surface or within a material, the variable "N_o" is used for this purpose. To find this quantity, eq 3 which is related to the occupation of specific sites within the material was utilized. It implies that by using this equation and the variable "N_o", one can calculate or determine the number of sorbed molecules. This calculation would depend on the actual content of eq 3 and the context in which it is being used.

$$Q_a = n_{ms}N_o \quad (10)$$

Equation 10 shows how the number of sorbed molecules is related to the number of available sites. This equation implies that the quantity of sorbed molecules is directly proportional to the number of available sites (more available sites generally lead to more sorption) and that plays a role in determining the extent of sorption, likely by defining the efficiency of the sorption process or the characteristics of the surface and the sorbing molecules. By utilizing eqs 2 and 3 the resultant equation takes the form as[53]

$$N_O = \left[e^{\beta(\varepsilon_1+\mu)} + \frac{2e^{\beta(\varepsilon_1+\varepsilon_2+2\mu)}(1 - e^{\beta(\varepsilon_2+\mu)N_L})}{(1 - e^{\beta(\varepsilon_2+\mu)})} - \frac{e^{\beta(\varepsilon_1+\varepsilon_2+2\mu)}N_L e^{\beta(\varepsilon_2+\mu)N_L}}{(1 - e^{\beta(\varepsilon_2+\mu)})} + \frac{e^{\beta(\varepsilon_1+\varepsilon_2+2\mu)}(1 - e^{\beta(\varepsilon_2+\mu)N_L})e^{\beta(\varepsilon_2+\mu)}}{(1 - e^{\beta(\varepsilon_2+\mu)})^2}\right] \Big/ \left[1 + e^{\beta(\varepsilon_1+\mu)} + \frac{e^{\beta(\varepsilon_1+\varepsilon_2+2\mu)}(1 - e^{\beta(\varepsilon_2+\mu)N_L})}{(1 - e^{\beta(\varepsilon_2+\mu)})}\right] \quad (11)$$

The following equation described the energy of adsorbed molecules on binding sites and determined the number of these site occupations using eq 5 and information related to chemical potentials. To rule out the interaction of molecules with binding sites on a surface of NC, these binding sites are locations where molecules can attach or be adsorbed. The energy associated with the adsorption process is important for understanding how molecules are held in place on these binding sites. The resultant equation is as follows

https://doi.org/10.1021/acsomega.4c01540
ACS Omega 2024, 9, 23873−23891

$$N_O = D_{sr}\left[e^{\beta(\varepsilon_{1am}+\mu_m)^{n_{ms}}} + \frac{2e^{\beta(\varepsilon_{1am}+\varepsilon_{2am}+2\mu_m)^{n_{ms}}}(1 - e^{\beta(\varepsilon_{2am}+\mu_m)^{n_{ms}N_L}})}{(1 - e^{\beta(\varepsilon_{2am}+\mu_m)^{n_{ms}}})} - \frac{e^{\beta(\varepsilon_{1am}+\varepsilon_{2am}+2\mu_m)^{n_{ms}}}N_L e^{\beta(\varepsilon_{2am}+\mu_m)^{n_{ms}N_L}}}{(1 - e^{\beta(\varepsilon_{2am}+\mu_m)^{n_{ms}}})} + \frac{e^{\beta(\varepsilon_{1am}+\varepsilon_{2am}+2\mu_m)^{n_{ms}}}(1 - e^{\beta(\varepsilon_{2am}+\mu_m)^{n_{ms}N_L}})e^{\beta(\varepsilon_{2am}+\mu_m)^{n_{ms}}}}{(1 - e^{\beta(\varepsilon_{2am}+\mu_m)^{n_{ms}}})^2}\right] \Bigg/ \left[1 + e^{\beta(\varepsilon_{1am}+\mu_m)^{n_{ms}}} + \frac{e^{\beta(\varepsilon_{1am}+\varepsilon_{2am}+2\mu_m)}(1 - e^{\beta(\varepsilon_{2am}+\mu_m)^{n_{ms}N_L}})}{(1 - e^{\beta(\varepsilon_{2am}+\mu_m)^{n_{ms}}})}\right] \quad (12)$$

Where $P_{hs1} = k_B T Z_g e^{-\beta\varepsilon}{}_{1am}$ and $P_{hs2} = k_B T Z_g e^{-\beta\varepsilon}{}_{2am}$ and $e\beta\mu_m$ is substituted by $\frac{\beta P}{Z_g}$ in eq 12. eq 11 contains the necessary mathematical relationships for calculating the number of molecules occupying these binding sites. This calculation also requires information related to chemical potentials. Chemical potentials are a concept from thermodynamics that describes the potential energy of a species in a system, and they play a crucial role in understanding how molecules interact with surfaces and materials.[53,56]

$$Q_a = n_{ms}\cdot D_{sr}\left[-\frac{2\left(\frac{P}{P_{hs1}}\right)^{2n_{ms}}}{\left(1 - \left(\frac{P}{P_{hs1}}\right)^{n_{ms}}\right)} + \frac{\left(\frac{P}{P_{hs1}}\right)^{n_{ms}}\left(1 - \left(\frac{P}{P_{hs1}}\right)^{2n_{ms}}\right)}{\left(1 - \left(\frac{P}{P_{hs1}}\right)^{n_{ms}}\right)^2} + \frac{2\left(\frac{P}{P_{hs1}}\right)^{n_{ms}}\left(\frac{P}{P_{hs2}}\right)^{n_{ms}}\left(1 - \left(\frac{P}{P_{hs2}}\right)^{(n_m N_L)}\right)}{\left(1 - \left(\frac{P}{P_{hs2}}\right)^{n_{ms}}\right)} - \frac{\left(\frac{P}{P_{hs1}}\right)^{n_{ms}}\left(\frac{P}{P_{hs2}}\right)^{n_{ms}}\left(\frac{P}{P_{hs2}}\right)^{(n_{ms}N_L)}N_L}{\left(1 - \left(\frac{P}{P_{hs2}}\right)^{n_{ms}}\right)} + \frac{\left(\frac{P}{P_{hs1}}\right)^{n_{ms}}\left(\frac{P}{P_{hs2}}\right)^{(2n_{ms})}\left(1 - \left(\frac{P}{P_{hs2}}\right)^{(n_{ms}N_L)}\right)}{\left(1 - \left(\frac{P}{P_{hs2}}\right)^{n_{ms}}\right)^2}\right] \Bigg/ \left[\frac{\left(1 - \left(\frac{P}{P_{hs1}}\right)^{2n_{ms}}\right)}{\left(1 - \left(\frac{P}{P_{hs1}}\right)^{n_{ms}}\right)} + \frac{\left(\frac{P}{P_{hs1}}\right)^{n_{ms}}\left(\frac{P}{P_{hs2}}\right)^{n_{ms}}\left(1 - \left(\frac{P}{P_{hs2}}\right)^{(n_{ms}N_L)}\right)}{\left(1 - \left(\frac{P}{P_{hs2}}\right)^{n_{ms}}\right)}\right] \quad (13)$$

3.2.1.1. Monolayer MSE. There are specific receptor sites referred to as D_{sr} receptor sites, which can adsorb a variable number of ions. Each receptor site can either be unoccupied (Ns = 0) or occupied (Ns = 1), and this binary occupancy state is central to the model's representation. The parameter "Ns" represents the number of ions adsorbed at a particular receptor site. The PF for a single receptor site is expressed by the following equation, which is a mathematical representation of the probability of different occupancy states (Knani et al., 2007)[59]

$$z_{gc} = \sum_{N_s=0,1} e^{-\beta(-\varepsilon-\mu)N_s} = 1 + e^{\beta(\varepsilon+\mu)} \quad (14)$$

Here, "z_{gc}" is the PF, and "β" represents the inverse of the thermal energy (kT), with "k" being the Boltzmann constant and "T" being the temperature. While "ε" is the energy associated with adsorption, and "μ" is the chemical potential of the adsorbed species. The summation ($\sum$) considers both occupancy states (Ns = 0 and Ns = 1) and calculates the probabilities associated with each state.

The adsorbed capacity (Q_a), which represents the total amount of adsorbate adsorbed on the surface, is determined by the product of the number of available receptor sites (n_{ms}) and the average occupancy per site (N_o). The half-saturation pressure ($P_{hs_{1/2}}$) is a crucial parameter in this equation, denoting the pressure at which approximately half of the receptor sites are occupied by adsorbate. The equation for the adsorbed capacity is given as follows

$$Q_a = n_{ms}N_o = \frac{n_{ms}D_{sr}}{\left(1 + \left(\frac{P_{hs1/2}}{P}\right)^{n_{ms}}\right)} \quad (15)$$

In this equation, "P" is the pressure, n_{ms} is the number of available receptor sites, and "D_{sr}" represents the number of ions that can be adsorbed by each receptor site. The equation considers the competition between the adsorption process and the pressure, ultimately determining the adsorbed capacity as a function of pressure and the characteristics of the adsorbent surface.

This model is valuable for understanding and predicting adsorption behavior in systems where receptor sites may have variable affinities for adsorbates and helps elucidate the relationship between pressure, occupancy of receptor sites, and adsorbed capacity. It was initially assumed that all receptor sites on the adsorbent surface are identical. This assumption simplifies the mathematical description of the adsorption process and serves as a fundamental basis for the model. It is important to note that receptor sites on a surface may have varying affinities for adsorbates, but this model assumes uniformity for the sake of simplicity and to establish a foundational framework for analysis.

3.2.1.2. Double Layer Model with Two Energies. In the process of constructing a mathematical model, a fundamental assumption is made, wherein it is postulated that the energy associated with the adsorption of the first layer of particles (denoted as $-\varepsilon_1$) is distinct from the energy related to the adsorption of the second layer of particles (denoted as $-\varepsilon_2$). This distinction in energies implies that when Cu^{2+} directly adheres to the surface of the adsorbent material, it forms stronger bonds compared to Cu^{2+} that has already been adsorbed in prior layers. This differentiation in binding energies is of critical importance in understanding the behavior of adsorbed species on the surface.

To delve deeper into this concept, one can consider the PF, a key mathematical expression used in SM to describe the distribution of energy states in a system. In this context, the PF can be expressed through a specific equation, which is a fundamental component of the mathematical model. This equation encapsulates the energetic disparities between the first and second adsorbed layers of Cu^{2+} on the adsorbent surface. It is important to highlight that this mathematical model is developed with the underlying assumption that a particular binding site, referred to as the D_{sr} binding site, is present. This assumption is based on the foundation for

https://doi.org/10.1021/acsomega.4c01540
ACS Omega 2024, 9, 23873−23891

understanding the adsorption phenomena of Cu^{2+} on the given adsorbent material.

The differentiation between the energies of the first and second adsorbed layers, along with the inclusion of the D_{sr} binding site in the model, allows for a more comprehensive and accurate representation of the adsorption process. It provides a means to describe and predict the behavior of Cu^{2+} on the adsorbent surface, considering the varying strengths of their interactions with the material. This mathematical model serves as a valuable tool for researchers and scientists in the field of adsorption chemistry, enabling them to gain insights into the mechanisms governing adsorption and potentially leading to the development of more effective adsorbent materials for various applications[59]

$$Z_{gc} = (1 + e^{\beta(\varepsilon_1+\mu)} + e^{\beta(\varepsilon_1+\varepsilon_2+2\mu)})^{D_{sr}} \quad (16)$$

The final eq takes the form as

$$Q_a = n_{ms}N_o = n_{ms}D_{sr}\frac{\left(\frac{P}{P_{hs1}}\right)^{n_{ms}} + 2\left(\frac{P}{P_{hs2}}\right)^{2n_{ms}}}{1 + \left(\frac{P}{P_{hs1}}\right)^{n_{ms}} + \left(\frac{P}{P_{hs2}}\right)^{2n_{ms}}} \quad (17)$$

In this equation, P_{hs1} and P_{hs2} refer to two critical values associated with a multilayer adsorption process, where a substance or molecules are being adsorbed onto a surface. They represent the half-saturation pressures for the first and second adsorbed layers.

P_{hs1} is the pressure at which the first layer of molecules or particles begins to cover approximately half of the available adsorption sites on the surface. When the pressure reaches P_{hs1}, about 50% of the adsorption sites on the surface are occupied by the first layer of adsorbate. Beyond this pressure, the first layer becomes more densely packed, and adsorption slows down.

P_{hs2} represents the pressure at which the second layer of molecules or particles begins to cover approximately half of the remaining available adsorption sites on the surface. Once Phs2 is reached, about 50% of the remaining adsorption sites are occupied by the second layer of adsorbate. The second layer of adsorption occurs on top of the first layer. These values, P_{hs1} and P_{hs2}, are crucial in the study of multilayer adsorption processes, as they help researchers understand the point at which each layer starts to form and the capacity of the adsorbent surface to accommodate additional layers of adsorbate.

3.2.2. Surface Biosorption Energy Analysis. Surface biosorption energy can be analyzed using SPF, which involves the application of thermodynamic principles to the study of systems composed of many particles. This can be done using techniques such as isothermal titration calorimetry or surface plasmon resonance. The SPF for analyzing surface biosorption energy involves considering the system as a collection of particles in thermal equilibrium with their environment.

The energy distribution on IER/CG was revealed to be unimodal when the biosorption energies were assessed at three different temperatures. It was found that the greatest peak intensity of IER/CG varied with sample temperature (Figure 4). Low Cu^{2+} biosorption binding site energies decreased with temperature because of an increase in energy distribution. The biosorption energy (E1 and E2) values in this experiment have a value of less than 23 kJ mol^{-1}. A small amount of biosorption interaction was seen on the analyzed adsorbent, indicating that the process was likely physisorption in nature. The optimal temperature ranges for the absorption of Cu^{2+} were found to be between 315 and 375 K.

3.2.3. In Vitro ACA. Numerous studies suggested that both the concentration of sulfate and 3,6-anhydrogalactose are responsible for ACA.[15,62,63] With the increase in the conc., the ACA increases in all the single CG and CG/IER (Figure 5).

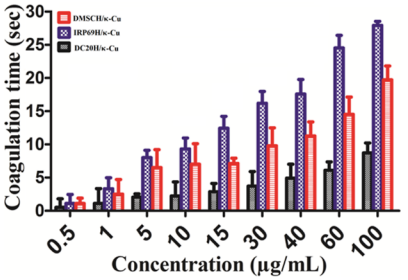

Figure 5. ACA of DMSCH/κ, DC20H/κ, and IRP69H/κ at different concentrations from 0.5 to 100 μg/mL.

These metal ions do have conc. dependent significant ACA. CG can form insoluble complexes when reacted with fibrinogen. However, the formation of precipitates was also evident for CG/IER alone. Fibrinogen causes opalescence which noticeably clears upon the addition of CG indicating the formation of insoluble complexes (Table 3). The insoluble

Table 3. Interaction of CG, CG/IER, IER Alone, and Their Metal Complexes with Fibrinogen (4 mg)[a]

s	concentrations (μg/mL)								
	0.5	1	5	10	15	30	40	60	100
κ-	+	+	+	+	0	0	0	0	0
κ-Cu	++	+	0	++					
IER-Cu	+	0	0						0
IER/κ-Cu	++	++	++	++		0	0	0	
DMSCH									
DC20H									
IRP69H									
heparin	136								

[a]+++ copious flocculated precipitate; + + flocculated precipitate; + finely dispersed precipitate; 0 = opalescence; - = clear solution.

complex formation is dependent on the SP making a complex with fibrinogen; this can take place even at a neutral pH of 7.[64] The difference in the time lapse of various coagula formations of the CG depends on its combination with different concentrations of Cu^{2+}. It was observed that IRP69H/κ- lowers the platelet count (PC) more effectively as compared to other samples due to the greater uptake of Cu^{2+}. Platelets are a type of blood cell that helps in the clotting process to stop bleeding. A decrease in PC refers to PC reduction. The phenomenon of agglutination is only possible when the PC remains unaffected, and a lower count does not support this phenomenon.

In Table 3, for CG, the interaction with fibrinogen is generally positive (++ or +) at lower concentrations but becomes less significant (0 or −) at higher concentrations. The metal complexes of CG/IER and IER show varied interactions with fibrinogen, with some concentrations leading to flocculated precipitates (++ or +), while others show no interaction (−). Other compounds like DMSCH, DC20H, and

https://doi.org/10.1021/acsomega.4c01540
ACS Omega 2024, 9, 23873−23891

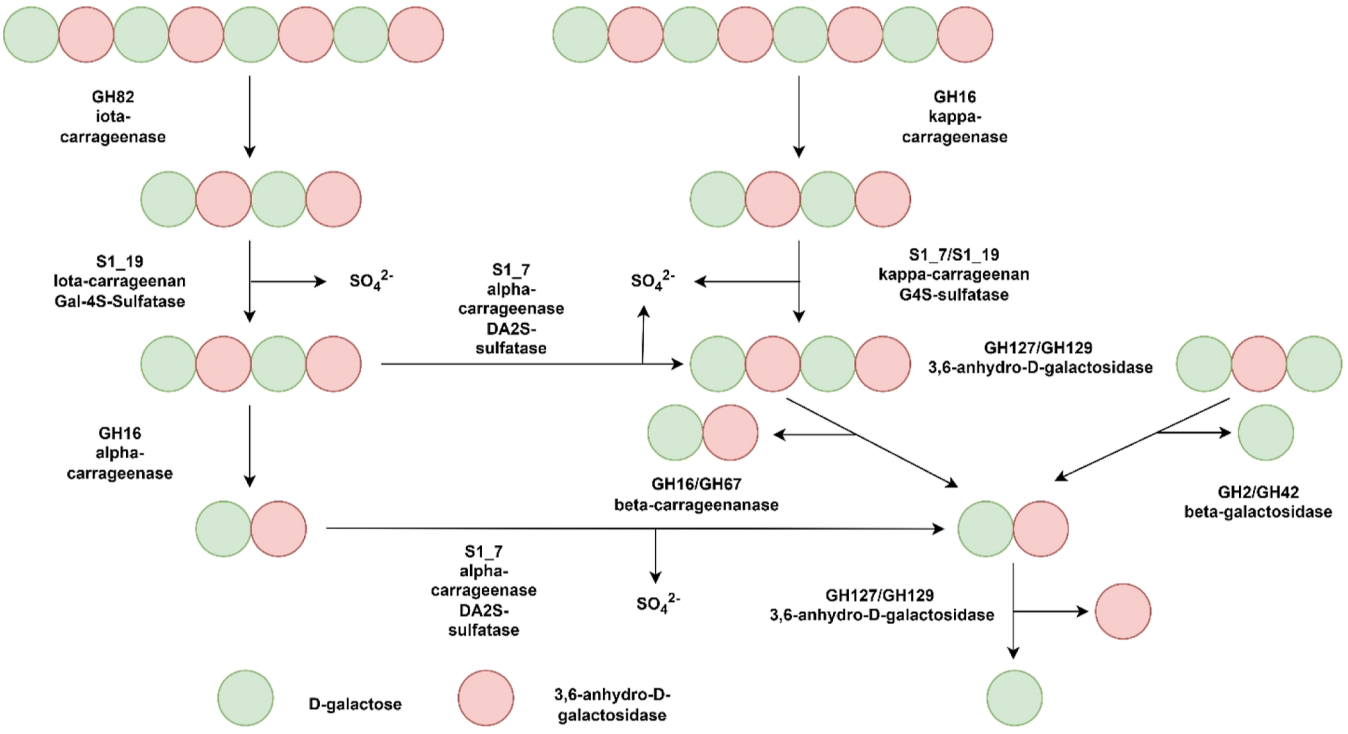

Figure 6. Degradation of carrageenan through enzymes during metabolism.

IRP69H show no observable interaction (−) with fibrinogen. Heparin forms a copious flocculated precipitate (+++), indicating a strong interaction with fibrinogen. The table provides insights into how different compounds and their metal complexes interact with fibrinogen at varying concentrations.

In this in vitro study comparing ACA, we assessed various compounds in comparison to heparin. The results of a prothrombin time experiment revealed that CG and CG/IER exhibited relatively low ACA (Figure 5). At a concentration of 100 μg/mL, DC20H/κ-Cu^{2+} exhibited an ACA of only 8 s. Notably, CG/IER showed higher ACA (Figure 5) compared to CG but lower compared to Cu^{2+}-complexed CG and CG/IER. Interestingly, our findings suggest that CG may predominantly affect the intrinsic pathways of the blood coagulation system rather than the extrinsic pathways.[15] Moreover, the fibrinogen complexation test indicated an interaction between CG and fibrinogen, possibly leading to the formation of insoluble complexes that could precipitate blood cells and platelets in the body.[65] Notably, the highest ACA of 38 s at a concentration of 100 μg/mL was observed with IRP69H/κ-Cu^{2+}. This indicates its potential as an effective anticoagulant in this context. Our results rank the compounds in terms of ACA as follows: DC20H/κ- < DMSCH/κ- < IRP69H/κ-.

The degradation of CG involves specific enzymes targeting its β-1,4-linkages to produce oligomeric neocarrabiose. Key enzymes include κ-, iota-, and lambda-carrageenases. These enzymes cleave the carrageenan chains, leading to the generation of smaller oligosaccharides. Additionally, CG requires desulfation for complete decomposition, facilitated by sulfatases. The degradation process involves sequential desulfation steps followed by enzymatic hydrolysis, ultimately resulting in the breakdown of CG into smaller fragments. Recent research has identified enzymes from various bacterial species, such as Pseudoalteromonas and Paraglaciecola, involved in CG degradation, highlighting the synergistic activity between sulfatases and glycoside hydrolases in this process[66] (Figure 6).

In our investigation of the agglutination phenomenon, a key observation is the critical role of PC. Agglutination is only possible when the PC remains unaffected, as a lower count does not support this phenomenon (Figure 7). Notably, the substance κ- exhibits an intriguing property—it does not lower the PC due to its structural characteristics, which prevent the

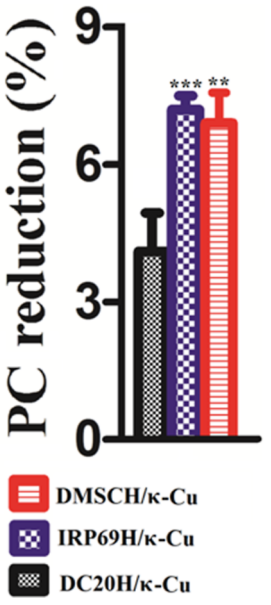

Figure 7. PC reduction by 1 mg/mL of DMSCH/κ-Cu, DC20H/κ-Cu, and IRP69H/κ-Cu. The IRP69H/κ- demonstrated the highest PC reduction at 1 mg/mL dose because of the highest Cu^{2+} intake.

https://doi.org/10.1021/acsomega.4c01540
ACS Omega 2024, 9, 23873−23891

Table 4. Brown, Green, and Red Algae as Adsorbents of Cu^{2+}[a]

metal	algal source	adsorbent	isotherm	q_{max} (mmol/g)	kinetics	pH	ref
Cu^{2+}	brown	Sargassum sp.	LAI	1.13	PSO	5.5	68
Cu^{2+}	green	Ulva fasciata	LAI	1.14	PSO	5.5	68
Cu^{2+}	green	Caulerpa lentillifera	LAI	0.08	IPD	5.0	69
Cu^{2+}	red	Gracillaria sp.	LAI	0.59	PSO	5.0	70
Cu^{2+}	brown	Fucus vesiculosus	LAI	1.66	PSO	5.0	71
Cu^{2+}	red	Asparagopsis armata	LAI	0.33	PSO	5.0	72
Cu^{2+}	red	Chondrus crispus	LAI	0.63	PSO	4.0	72
Cu^{2+}	brown	Fucus spiralis	LAI	1.0	PSO	4.0	72
Cu^{2+}	brown	Ascophyllum nodosum	LAI	0.91	PSO	4.0	72

[a]LAI—Langmuir adsorption isotherm, PSO—pseudo second order, IPD—intraparticle diffusion.

Table 5. ACA of CG and Cyclized CG

compound	species	carrageenan type	sulfate as SO_3Na (%)	molecular weight (kDa)	flexibility parameter	TT[c] (TT ratio relative to control the sample without a compound) concentration (μg/mL)				
						200	100	50	5	0.5
C1, C2, C3, C4	Gigartina skottsbergii	κ-/ι-	33.1, 31.4, 34.5, 35.3	75, 124, 73, 18	0.100	2.0, 2.1, 1.2, 1.0	1.5, 1.7, 1.3, 1.0	1.5, 1.5, 1.3, 1.0	1.0, 1.0, 1.0, 1.0	1.0, 1.0, 1.0, 1.0
C5, C6, C6	Gigartina skottsbergii	λ-	38.5	n.d., 83, 121	0.053	≥11.5	≥11.5 for all	3.6	1.4, 2.2, 2.1	1.3, 1.3, 1.4
								≥11.5, ≥11.5		
			40.0							
						n.d				
			39.2			n.d				
C7, C8	Gigartina skottsbergii	cyclized λ-	35.9, 35.8	66, 17	0.083	2.2, 1.5	2.0	1.2, 1.9	1.1, 1.0	1.1, 1.0
							1.3			
heparin			36						>11.5	>11.5

trapping of platelets. Consequently, lower agglutination is observed in the presence of κ-.[67]

Table 4 provides a comprehensive overview of Cu^{2+} adsorption by various algal sources using different adsorbents, along with the corresponding isotherm parameters, maximum adsorption capacity (q_{max}), kinetics, and pH conditions. Different algal species, categorized by color (brown, green, and red), such as Sargassum sp., Ulva fasciata,[68] Caulerpa lentillifera,[69] Gracillaria sp.,[70] Fucus vesiculosus,[71] Asparagopsis armata, Chondrus crispus, Fucus spiralis, and Ascophyllum nodosum,[72] were investigated for their Cu^{2+} adsorption potential. The adsorbent used was Langmuir adsorption isotherm (LAI), and the adsorption isotherm followed the pseudo-second-order (PSO) or the intraparticle diffusion (IPD) model. The pH conditions ranged from 4.0 to 5.5, indicating the influence of pH on Cu^{2+} adsorption onto algal biomass. These data provide valuable insights into the potential of different algal species as eco-friendly and cost-effective adsorbents for Cu^{2+} removal from aqueous solutions, aiding in environmental remediation efforts.

Table 5 presents data on the effect of different compounds on carrageenan properties, focusing on sulfate content, molecular weight, flexibility parameter, and transition temperature (TTc) relative to control samples. Compound C1, C2, C3, and C4, extracted from Gigartina skottsbergii, influenced κ-/ι-CG types, with sulfate content ranging from 31.4 to 35.3% and molecular weights between 18 and 124 kDa. Flexibility parameters varied from 1.0 to 2.1, while TTc ratios showed concentration-dependent effects. Compounds C5, C6, and C6, also from Gigartina skottsbergii, affected λ-CG, with sulfate contents ranging from 38.5 to 40.0%, and molecular weights between 83 and 121 kDa. Flexibility parameters and TTc ratios demonstrated concentration-dependent variations. Compounds C7 and C8, cyclized λ-carrageenans from Gigartina skottsbergii, exhibited sulfate contents of 35.8 to 35.9%, with molecular weights of 17 and 66 kDa, influencing flexibility and TTc ratios in a concentration-dependent manner. Heparin used as a reference displayed a sulfate content of 36%, with TTc ratios consistently greater than 11.5 across all concentrations, suggesting its distinct behavior compared to CG compounds.[68−72]

It is worth noting that even lower concentrations of CG were observed to be sufficient to cause precipitation. The findings indicate that CG does not exclusively form complexes with fibrinogen but also interacts with other clotting proteins. These interactions result in the formation of insoluble complexes between CG and other clotting proteins, potentially leading to embolism (Table 6).

Table 6 provides information on various algae species, including their division, flagella presence, isolation method, compound names, composition, algae type, glycosidic linkage, molecular weight (mw), and acetyl content. Grateloupia livida,[73] a red algae from the Phaeophyta division, exhibits compounds GLP-1, −2, and −3 composed mainly of galactose, with mw ranging from 3.36 to 60.4 kDa. Sargassum horneri,[74] another Phaeophyta species, has compounds SHP-80, −60, and −30, consisting of xylose and glucose, with mw ranging from 11.2 to 1.92 × 10^3 kDa. Sargassum aquifolium,[75] also Phaeophyta, contains xylose, galactose, fucose, glucuronic acid, and mannose, with α-L-fucopyranose or β-D-xylopyranose linkage at position 3. Enteromorpha clathrate,[18] green algae, has galactose, rhamnose, and arabinose, with partially sulfate

https://doi.org/10.1021/acsomega.4c01540
ACS Omega 2024, 9, 23873−23891

groups at the C3 position of 1,4-β-L-arabinose residues. Monostroma latissimum,[76] a Chlorophyta species, is composed of xylose, rhamnose, and glucose. Lastly, Codium divaricatum,[17] also Chlorophyta, contains glucose and galactose, with single (1 →)-β-D-galactopyranose units connected to the main chain at O4 locations and branch 1,3-β-D-galactopyranose residues.

We observed that heparin forms insoluble complexes when infused with thrombin, an effect attributed to sulfate groups present at various positions in its pentasaccharide structure.[20] This characteristic of heparin contributes to its ACA. CG, like heparin, contains sulfate groups at specific sites, suggesting the potential for ACA, as indicated in previous studies conducted either with isolated CG or degraded CG (Table 5).[77] However, an unexplored aspect in prior research is the impact of blending all three forms of CG, κ, λ, and ι, on the degree of sulfation and its potential influence on ACA. Furthermore, galactose-2-sulfate, a sulfate group unique to λ-CG, may also play a role in ACA. The extent and position of sulfation in CG (κ, λ, ι) may be critical factors influencing ACA (Table 6). Our study highlights the importance of sulfate groups in heparin and CG and their potential implications for ACA.

This study delves into the dynamic role of the CG/IER complex when combined with Cu^{2+} and its implications for ACA. Initially, it was hypothesized that higher sulfate content would lead to greater ACA; however, subsequent research revealed that sulfate content alone was insufficient evidence.[78] ACA is a multifaceted phenomenon influenced by a multitude of factors beyond sulfate content. CG has been shown to exhibit ACA through various mechanisms, including fibrin formation, the physiological resolution of anticoagulant pathways, and platelet activation.[15,78,79] Similarly, Cu^{2+} on its own[80] and as part of its complexes[30] is known to possess significant ACA. Deficiency of Cu^{2+} can result in clotting abnormalities and bleeding.[81] A proposed mechanism of ACA is illustrated in Figure 8.

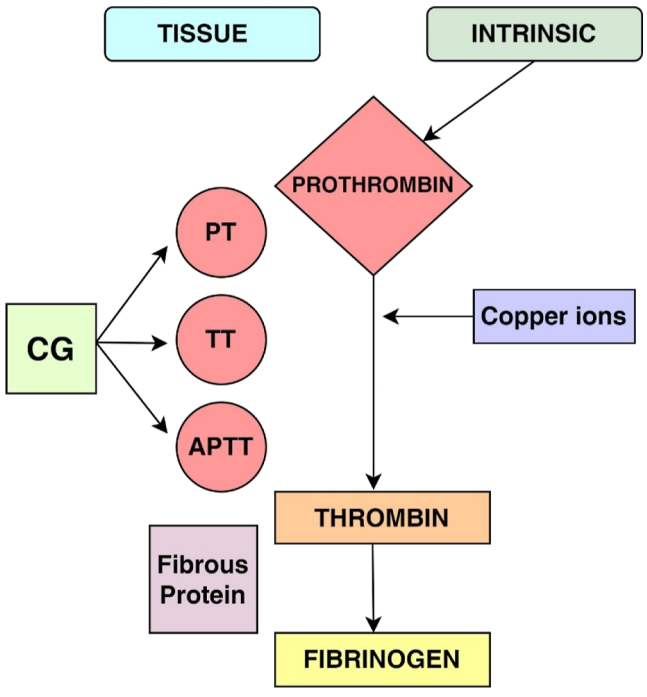

Figure 8. Proposed mechanism of ACA of CG and copper.

Table 6. ACA of SP[a]

species	division	flagella	method	name	composition	algae	glycosidic linkage	Mw (kDa)	ACA	ref
Grateloupia livida	phaeophyta	Absent	water	GLP-1, −2, −3	Gal	red		39.5, 60.4, 3.36	cell	73
Sargassum horneri	phaeophyta	Present	water	SHP-80, −60 and −30	Xyl, Glc	brown		11.2, 1.92 × 10^3, 1.58 × 10^3	cell	74
Sargassum aquifolium	phaeophyta	present	water		Xyl, Gal, Fuc, GlcA, Man	brown	α-L-Fucp or β-D-Xylp at position 3		cell	75
Enteromorpha clathrata			water	FEP	Gal, Rha, Arabinose (Ara), GlcA	green	1,4-β-L-Ara residues with partially sulfate groups at the C3-position	511	cell	18
Monostroma latissimum	chlorophyta	present	water		Xyl, Rha, Glc	green		55	cell	76
Codium divaricatum	chlorophyta	present	water	CP2−1	Glc and Galc	green	Single (1→)-β-D-Galp units that are connected to the main chain at O4 locations branch 1,3-β-D-Galp residues	37.9	cell	17

[a]Brown algae-fucoidan, alginate, red-algae-galactans, xylans, cellulose, green algae-β-mannans, β-xylans, cellulose hydroxyl−proline glucosides, Mw—molecular weight, ACA—ACA.

https://doi.org/10.1021/acsomega.4c01540
ACS Omega 2024, 9, 23873−23891

The presence of Cu^{2+} demonstrating the ACA confirms the hypothesis of Anderson et al.[78] that the ACA is not entirely dependent on the sulfate content. The Cu^{2+}-complexed CG mostly showed the highest ACA results.[67] For the blood clotting test 2 mg/kg of lambda-CG was found to be the highest; an increase to 5 and 6 mg/kg rendered it toxic which has been reported previously.[78]

Numerous factors are involved in the ACA of SP such as the degree of sulfation, hydrophobic pockets, the position of the sulfate group, glycosidic linkages, and molecular weight. While oversulfation makes AC out of neutral polysaccharides that have no biological functions.[82] The sulfate group's position, not their degree of substitution, has the greatest effect on the ACA. The most beneficial site for substitution among them is C-2 of 3,6-anhydro-β-d-Galp, whereas the least advantageous is C-6 of β-d-Galp. The highest potential sulfated monosaccharide units for ACA should have two sulfate groups, a glycosidic bond on the pyranose ring, and C-2, C-3, and C-4 in the configurations 2S, 3S, 4R for rhamnose, 2S, 3R, 4R or 2R, 3S, 4S for arabinose, fucose, and galactose. The nonspecific polar interaction between the negatively and positively charged groups in the polysaccharide and protein is thought to be instrumental in the formation of the sulfated polysaccharide/protein complex, and short-range interactions are thought to further stabilize the complex.[83]

The variations in ACA of SP may be explained by their different structural orientation and the possibility that a single molecule may have more than one target protease.[84] Despite having a high concentration of sulfate groups, members of the κ- and ι- families only exhibit weak ACA.[63] This suggests that the loss of the sulfate group on the B−C-6 units or the transition from a relatively rigid, ribbon-like conformation to a more flexible helix was detrimental to the ACA. The latter idea is supported by the fact that the ACA is unaffected by the presence or absence of the 6-sulfate in (1 → 4)-linked polysaccharides.[69] The structural foundation for the ACA of λ would be the pattern of sulfation on C-2 of the A-unit and C-6 of the B-unit on a backbone with limited A → B flexibility that facilitates the ordered conformation.[67] The in vitro addition of Cu^{2+} sulfate (300−1000 μg/mL) resulted in a considerably reduced thrombin time.[31]

CG are polyanionic polymers with highly selective cationic chelating activity, making them ideal for metal uptake.[29] Cu^{2+} had a substantial impact in an in vitro experiment where the blood coagulation time increased greatly when the concentration of Cu^{2+} was increased.[80] Polysaccharides containing an intact sulfate functional group outperformed polymers of equivalent molecular weight. Furthermore, it appears to be more powerful than the total degree of sulfation in which this pattern was disrupted by partial desulfation. As previously reported studies,[15,63,82] the basis of the ACA of CG seems to be an antithrombic.[85]

3.3. Conclusions. This study underscores the significance of CG/IER complexes in their ability to bind to metals, potentially opening avenues for therapeutic cation administration. It appears that the sulfate content is a likely contributor to the in vitro ACA observed in κ-. The formation of insoluble complexes through the complexation of fibrinogen with the samples further emphasizes their potential to influence coagulation processes. The results reveal a specific order of ACA among the samples, with DC20H/κ- < DMSCH/κ- < IRP69H/κ-. Notably, IRP69H/κ- exhibits a higher capacity for Cu^{2+} uptake compared to the other two NCs, shedding light on the role of metal binding in their anticoagulant properties. It is worth noting that Cu^{2+}, an essential trace mineral, has demonstrated anticoagulant properties by inhibiting blood clot formation. However, the research on the potential ACA of Cu^{2+} is still in its early stages, warranting further investigation to fully comprehend its effects. It is important to acknowledge that the effects of Cu^{2+} on blood clotting are multifaceted and can depend on various factors, including Cu^{2+} concentration and the presence of other substances or metals in the blood. In the pursuit of a comprehensive understanding of these complex interactions, future research will be essential to unlock the full therapeutic potential of CG/IER complexes and their metal-binding properties.

3.3.1. Strengths of the Study.

1. This study comprised the novel surface-modified nanocomposite IER and CG to investigate the biosorption of Cu^{2+}. While biosorption studies are not uncommon, the specific use of these blends in conjunction with ANN and SPF adds a unique dimension to our research.
2. The MLP approach allows for the prediction of material adsorption capacities based on various input factors such as temperature, pH, dose, surface area, and adsorbate concentration. The use of MLP in adsorption studies is innovative and offers a potential avenue for optimizing adsorption processes.
3. The study introduces the use of SPF to model the behavior of complex adsorption systems, particularly focusing on the steric and energetic interpretations of Cu^{2+} biosorption. By combining both interpretations, the SPF model provides a comprehensive understanding of the adsorption process, enabling the prediction of adsorption capacity under different conditions.
4. The study explored the potential for tailoring the properties of these materials for specific applications such as metal ion removal.
5. In addition to the biosorption studies, the research included an in vitro investigation of the ACA. This aspect added a multidisciplinary dimension to the study, showcasing the versatility of the materials under investigation.

3.3.2. Limitations of the Study. While the study contributes significantly to the understanding of adsorption processes and materials, it is essential to recognize its limitations and areas for improvement to guide future research efforts effectively.

1. The ANN and SPF models rely on certain assumptions and simplifications that may not fully capture the complexity of real-world systems. For example, the MLP model may oversimplify the interactions between input variables and adsorption capacity, leading to potential inaccuracies in predictions and requiring laborious analysis to correctly predict the data.
2. The findings of the study may be specific to the materials, conditions, and experimental setup used in the research. As such, they may not be directly applicable to other adsorbent materials or environmental conditions. Generalizing the results to broader contexts requires careful consideration of potential variations and uncertainties. This requires expertise, and generally such research activities could not be performed easily.

https://doi.org/10.1021/acsomega.4c01540
ACS Omega 2024, 9, 23873−23891

3. Further investigations into the biological and biomedical implications of the materials used, as well as their potential toxicity or biocompatibility, could provide a more comprehensive understanding of their applications in biomedical fields.

3.3.3. Future Recommendations.

1. The study highlights the potential of using ANN and SPF for modeling and predicting adsorption processes. Future research could focus on refining these models to improve their accuracy and efficiency in predicting adsorption capacities under various conditions. This could involve experimenting with different network architectures for MLP or incorporating additional factors into the SPF model to enhance its predictive capabilities.
2. While the study focuses on IER and CG, there is scope for exploring other types of adsorbent materials with potentially superior adsorption properties. Future research could investigate the synthesis and characterization of novel materials and assess their suitability for applications in adsorption processes, such as wastewater treatment or pollutant removal.
3. The study demonstrates the integration of experimental techniques with computational modeling to gain insights into adsorption phenomena. Future research could further leverage this interdisciplinary approach by combining experimental data with advanced computational simulations, such as molecular dynamics simulations or density functional theory calculations, to deepen our understanding of adsorption mechanisms at the molecular level.
4. The insights gained from the study have implications beyond adsorption research, particularly in environmental remediation and biomedical applications. Future investigations could explore the use of the developed models and materials for addressing real-world challenges, such as water purification, drug delivery, or biomedical implants.
5. Collaborations with industry partners or interdisciplinary research teams could facilitate the translation of research findings into practical applications.
6. Our study highlights the complex nature of ACA and the involvement of multiple factors beyond sulfate content in CG/IER-Cu^{2+} complexes. Advanced research is needed to elucidate the intricate mechanisms that govern ACA. Further exploration of the degree and location of sulfation in CG, especially when blending all three forms, may yield valuable insights into its anticoagulant properties.
7. Our study sheds light on the complex interplay between PC, agglutination, and the interactions of CG with various clotting proteins, emphasizing the need for further research in this area as well.

AUTHOR INFORMATION

Corresponding Author

Saad Salman − *Department of Pharmacy, CECOS University of IT and Emerging Sciences, Hayatabad, Peshawar, Khyber Pakhtunkhwa 25000, Pakistan;* Present Address: Department of Biological Sciences, Kongju National University, Gongju 314-701, Republic of Korea; orcid.org/0000-0001-6592-9812; Phone: +92 3335690747; Email: saadirh@gmail.com, saad.salman@cecos.edu.pk

Authors

Sana Haider − *Department of Pharmacy, University of Peshawar, Peshawar 25120, Pakistan*

Sami Ullah − *Department of Pharmacy, University of Peshawar, Peshawar 25120, Pakistan*

Mohsin Kazi − *Department of Pharmaceutics, College of Pharmacy, King Saud University, Riyadh 11451, Saudi Arabia*

Fouzia Qamar − *Department of Biology, Lahore Garrison University, Lahore 54000, Pakistan*

Tariq Siddique − *Faculty of Pharmacy, Ibadat International University, Islamabad 44000, Pakistan*

Rubia Anwer − *Faculty of Pharmacy, Ibadat International University, Islamabad 44000, Pakistan;* orcid.org/0000-0002-9640-5912

Saeed Ahmad Khan − *Sharjah Institute of Medical Research, Dubai 500001, United Arab Emirates; Department of Pharmacy, Kohat University of Science and Technology, Kohat 26000, Pakistan;* Present Address: Research Institute of Medical and Health Sciences, University of Sharjah, Sharjah 211, United Arab Emirates; orcid.org/0000-0001-5606-2719

Complete contact information is available at: https://pubs.acs.org/10.1021/acsomega.4c01540

Author Contributions

S.S. conceived the idea; S.H. conducted the research; S.H. and S.S. wrote the initial draft; S.U., M.K., and S.A.K. analyzed the data; and F.Q., T.S., and R.A. drafted/edited the final manuscript and helped with the revisions.

Notes

The Ethical Committee of the CECOS University of IT & Emerging Sciences approved the study involving animals (Reg. no. PHARM/RS-0053-23).

The authors declare no competing financial interest.

ACKNOWLEDGMENTS

The authors would like to extend their sincere appreciation to the Researchers Supporting Project Number (RSP2024R301), King Saud University, Riyadh, Saudi Arabia.

REFERENCES

(1) Kakuda, M.; Matsuzaki, S.; Ueda, Y.; Shiomi, M.; Matsuzaki, S.; Kimura, T.; Fujita, M.; Egawa-Takata, T.; Kobayashi, E.; Serada, S.; et al. Copper ions are novel therapeutic agents for uterine leiomyosarcoma. *Am. J. Obstet. Gynecol.* **2020**, *222* (1), 64.e1−64.e16.

(2) Oliveri, V. Biomedical applications of copper ionophores. *Coord. Chem. Rev.* **2020**, *422*, 213474.

(3) Baldari, S.; Di Rocco, G.; Toietta, G. Current Biomedical Use of Copper Chelation Therapy. *Int. J. Mol. Sci.* **2020**, *21* (3), 1069.

(4) Latorre, M.; Troncoso, R.; Uauy, R. Biological Aspects of Copper. In *Clinical and Translational Perspectives on WILSON DISEASE*; Elsevier, 2019; pp 25−31.

(5) Xu, A.; Chang, H.; Xu, Y.; Li, R.; Li, X.; Zhao, Y. Applying artificial neural networks (ANNs) to solve solid waste-related issues: A critical review. *Waste Manag.* **2021**, *124*, 385−402.

(6) Bhagat, S. K.; Pyrgaki, K.; Salih, S. Q.; Tiyasha, T.; Beyaztas, U.; Shahid, S.; Yaseen, Z. M. Prediction of copper ions adsorption by attapulgite adsorbent using tuned artificial intelligence model. *Chemosphere* **2021**, *276*, 130162.

(7) Selim, A. Q.; Sellaoui, L.; Ahmed, S. A.; Mobarak, M.; Mohamed, E. A.; Lamine, A. B.; Erto, A.; Bonilla-Petriciolet, A.; Seliem, M. K. Statistical physics-based analysis of the adsorption of Cu2+ and Zn2+ onto synthetic cancrinite in single-compound and binary systems. *J. Environ. Chem. Eng.* **2019**, *7* (4), 103217.
(8) Salman, S.; Asghar, S.; Khan, I. U.; Khalid, S. H.; Shah, F. H.; Usman, M. Equilibrium, kinetics, thermodynamics and docking studies of Cu 2 + ion adsorption over ion-exchange resin and kappa carrageenan blends in blood samples. *Pak. J. Pharm. Sci.* **2020**, *33*, 795−803. Published online
(9) Idrees, F.; Sibtain, F.; Dar, M. J.; Shah, F. H.; Alam, M.; Hussain, I.; Kim, S. J.; Idrees, J.; Khan, S. A.; Salman, S. Copper biosorption over green silver nanocomposite using artificial intelligence and statistical physics formalism. *J. Clean. Prod.* **2022**, *374*, 133991.
(10) Amrhar, O.; El Gana, L.; Mobarak, M. Calculation of adsorption isotherms by statistical physics models: a review. *Environ. Chem. Lett.* **2021**, *19* (6), 4519−4547.
(11) Campo, V. L.; Kawano, D. F.; Silva, D. B. d.; Carvalho, I. Carrageenans: Biological properties, chemical modifications and structural analysis - A review. *Carbohydr. Polym.* **2009**, *77* (2), 167−180.
(12) Guo, Z.; Wei, Y.; Zhang, Y.; Xu, Y.; Zheng, L.; Zhu, B.; Yao, Z. Carrageenan oligosaccharides: A comprehensive review of preparation, isolation, purification, structure, biological activities and applications. *Algal Res.* **2022**, *61*, 102593.
(13) van de Velde, F. Structure and function of hybrid carrageenans. *Food Hydrocolloids* **2008**, *22* (5), 727−734.
(14) Rhein-Knudsen, N.; Ale, M. T.; Ajalloueian, F.; Yu, L.; Meyer, A. S. Corrigendum to "Rheological properties of agar and carrageenan from Ghanaian red seaweeds" [Food Hydrocolloids 63 (2017) 50−58]. *Food Hydrocolloids* **2018**, *81*, 284−285.
(15) Silva, F. R. F.; Dore, C. M. P. G.; Marques, C. T.; Nascimento, M.; Benevides, N.; Rocha, H.; Chavante, S.; Leite, E. Anticoagulant activity, paw edema and pleurisy induced carrageenan: Action of major types of commercial carrageenans. *Carbohydr. Polym.* **2010**, *79* (1), 26−33.
(16) Kang, J.; Jia, X.; Wang, N.; Xiao, M.; Song, S.; Wu, S.; Li, Z.; Wang, S.; Cui, S. W.; Guo, Q. Insights into the structure-bioactivity relationships of marine sulfated polysaccharides: A review. *Food Hydrocolloids* **2022**, *123*, 107049.
(17) Li, N.; Mao, W.; Yan, M.; Liu, X.; Xia, Z.; Wang, S.; Xiao, B.; Chen, C.; Zhang, L.; Cao, S. Structural characterization and anticoagulant activity of a sulfated polysaccharide from the green alga Codium divaricatum. *Carbohydr. Polym.* **2015**, *121*, 175−182.
(18) Qi, X.; Mao, W.; Gao, Y.; Chen, Y.; Chen, Y.; Zhao, C.; Li, N.; Wang, C.; Yan, M.; Lin, C.; et al. Chemical characteristic of an anticoagulant-active sulfated polysaccharide from Enteromorpha clathrata. *Carbohydr. Polym.* **2012**, *90* (4), 1804−1810.
(19) Wang, P.; Chi, L.; Zhang, Z.; Zhao, H.; Zhang, F.; Linhardt, R. J. Heparin: An old drug for new clinical applications. *Carbohydr. Polym.* **2022**, *295*, 119818.
(20) Bal dit Sollier, C.; Dillinger, J. G.; Drouet, L. Anticoagulant activity and pleiotropic effects of heparin. *JMV* **2020**, *45* (3), 147−157.
(21) Melo, F. R.; Pereira, M. S.; Foguel, D.; Mourão, P. A. Antithrombin-mediated Anticoagulant Activity of Sulfated Polysaccharides: DIFFERENT MECHANISMS FOR HEPARIN AND SULFATED GALACTANS*. *J. Biol. Chem.* **2004**, *279* (20), 20824−20835.
(22) Rahelivao, M. P.; Gruner, M.; Andriamanantoanina, H.; Andriamihaja, B.; Bauer, I.; Knölker, H. J. Red Algae (Rhodophyta) from the Coast of Madagascar: Preliminary Bioactivity Studies and Isolation of Natural Products. *Mar. Drugs* **2015**, *13* (7), 4197−4216.
(23) dos Santos-Fidencio, G. C.; Gonçalves, A. G.; Noseda, M. D.; Duarte, M. E. R.; Ducatti, D. R. B. Effects of carboxyl group on the anticoagulant activity of oxidized carrageenans. *Carbohydr. Polym.* **2019**, *214*, 286−293.
(24) Zia, K. M.; Tabasum, S.; Nasif, M.; Sultan, N.; Aslam, N.; Noreen, A.; Zuber, M. A review on synthesis, properties and applications of natural polymer based carrageenan blends and composites. *Int. J. Biol. Macromol.* **2017**, *96*, 282−301.
(25) Karavas, E.; Koutris, E.; Papadopoulos, A. G.; Sigalas, M. P.; Nanaki, S.; Papageorgiou, G. Z.; Achilias, D. Z.; Bikiaris, D. N. Application of density functional theory in combination with FTIR and DSC to characterise polymer drug interactions for the preparation of sustained release formulations between fluvastatin and carrageenans. *Int. J. Pharm.* **2014**, *466* (1−2), 211−222.
(26) Brychcy, E.; Malik, M.; Drożdżewski, P.; Król, Ż.; Jarmoluk, A. Physicochemical and Antibacterial Properties of Carrageenan and Gelatine Hydrosols and Hydrogels Incorporated with Acidic Electrolyzed Water. *Polymer* **2015**, *7* (12), 2638−2649.
(27) Stamboroski, S.; Boateng, K.; Lierath, J.; Kowalik, T.; Thiel, K.; Köppen, S.; Noeske, P. L. M.; Brüggemann, D. Influence of Divalent Metal Ions on the Precipitation of the Plasma Protein Fibrinogen. *Biomacromolecules* **2021**, *22* (11), 4642−4658.
(28) Lages, B.; Stivala, S. S. Copper ion binding and heparin interactions of human fibrinogen. *Biopolymers* **1973**, *12* (5), 961−974.
(29) Shashidharagowda, H.; Mathad, S.; Malladi, S.; Gubbiveeranna, V.; Patil, A.; Khan, A.; Rub, M. A.; Asiri, A.; et al. Sol−Gel Co-Precipitation Synthesis, Anticoagulant and Anti-Platelet Activities of Copper-Doped Nickel Manganite Nanoparticles. *Gels* **2021**, *7* (4), 269.
(30) Flores-García, M.; Fernández-G, J. M.; Busqueta-Griera, C.; Gómez, E.; Hernández-Ortega, S.; Lamothe-Flores, J. C. D.; Gómez-Vidales, V.; Mejía-Domínguez, A. M.; Anglés-Cano, E.; de la Peña-Díaz, A. New Copper Compounds with Antiplatelet Aggregation Activity. *Med. Chem.* **2019**, *15* (8), 850−862.
(31) Abou-Shady, E. A.; Farrag, H. E.; el-Damarawy, N. A.; Mohamed, F. A.; Kamel Aam, A. M. In vitro effects of trace elements on blood clotting and platelet function. A-Iron, copper, and gold. *J. Egypt Public Health Assoc.* **1991**, *66* (1−2), 21−48.
(32) Demirbas, E.; Dizge, N.; Sulak, M. T.; Kobya, M. Adsorption kinetics and equilibrium of copper from aqueous solutions using hazelnut shell activated carbon. *Chem. Eng. J.* **2009**, *148* (2−3), 480−487.
(33) Madhava Rao, M.; Ramesh, A.; Purna Chandra Rao, G.; Seshaiah, K. Removal of copper and cadmium from the aqueous solutions by activated carbon derived from Ceiba pentandra hulls. *J. Hazard. Mater.* **2006**, *129* (1−3), 123−129.
(34) Song, J.; Zhang, R.; Li, K.; Li, B.; Tang, C. Adsorption of Copper and Zinc on Activated Carbon Prepared from Typha latifolia L. *Clean: Soil, Air, Water* **2015**, *43* (1), 79−85.
(35) Liu, Z.; Wei, Y. K_2CO_3-Activated Pomelo Peels as a High-Performance Adsorbent for Removal of Cu(II): Preparation, Characterization, and Adsorption Studies. Alsohaimi IH, ed. *J. Chem.* **2021**, *2021*, 9940577.
(36) Sabela, M. I.; Kunene, K.; Kanchi, S.; Xhakaza, N. M.; Bathinapatla, A.; Mdluli, P.; Sharma, D.; Bisetty, K. Removal of copper (II) from wastewater using green vegetable waste derived activated carbon: An approach to equilibrium and kinetic study. *Arab J. Chem.* **2019**, *12* (8), 4331−4339.
(37) Kazemipour, M.; Ansari, M.; Tajrobehkar, S.; Majdzadeh, M.; Kermani, H. R. Removal of lead, cadmium, zinc, and copper from industrial wastewater by carbon developed from walnut, hazelnut, almond, pistachio shell, and apricot stone. *J. Hazard. Mater.* **2008**, *150* (2), 322−327.
(38) Demiral, H.; Güngör, C. Adsorption of copper(II) from aqueous solutions on activated carbon prepared from grape bagasse. *J. Clean. Prod.* **2016**, *124*, 103−113.
(39) Imamoglu, M.; Tekir, O. Removal of copper (II) and lead (II) ions from aqueous solutions by adsorption on activated carbon from a new precursor hazelnut husks. *Desalination* **2008**, *228* (1−3), 108−113.
(40) Shawabkeh, R. A.; Rockstraw, D. A.; Bhada, R. K. Copper and strontium adsorption by a novel carbon material manufactured from pecan shells. *Carbon* **2002**, *40* (5), 781−786.
(41) Kalavathy, M. H.; Karthikeyan, T.; Rajgopal, S.; Miranda, L. R. Kinetic and isotherm studies of Cu(II) adsorption onto H3PO4-

https://doi.org/10.1021/acsomega.4c01540
ACS Omega 2024, 9, 23873−23891

activated rubber wood sawdust. *J. Colloid Interface Sci.* **2005**, *292* (2), 354−362.
(42) Gao, X.; Wu, L.; Xu, Q.; Tian, W.; Li, Z.; Kobayashi, N. Adsorption kinetics and mechanisms of copper ions on activated carbons derived from pinewood sawdust by fast H3PO4 activation. *Environ. Sci. Pollut. Res.* **2018**, *25* (8), 7907−7915.
(43) Wilson, K.; Yang, H.; Seo, C. W.; Marshall, W. E. Select metal adsorption by activated carbon made from peanut shells. *Bioresour. Technol.* **2006**, *97* (18), 2266−2270.
(44) Kobya, M.; Demirbas, E.; Senturk, E.; Ince, M. Adsorption of heavy metal ions from aqueous solutions by activated carbon prepared from apricot stone. *Bioresour. Technol.* **2005**, *96* (13), 1518−1521.
(45) Özçimen, D.; Ersoy-Meriçboyu, A. Removal of copper from aqueous solutions by adsorption onto chestnut shell and grapeseed activated carbons. *J. Hazard. Mater.* **2009**, *168* (2−3), 1118−1125.
(46) Mahvi, A. H.; Balarak, D.; Bazrafshan, E. Remarkable reusability of magnetic Fe3O4-graphene oxide composite: a highly effective adsorbent for Cr(VI) ions. *Int. J. Environ. Anal. Chem.* **2023**, *103* (15), 3501−3521.
(47) Bazrafshan, E.; Sobhanikia, M.; Mostafapour, F. K.; Kamani, H.; Balarak, D. Chromium biosorption from aqueous environments by mucilaginous seeds of Cydonia oblonga: Kinetic and thermodynamic studies. *Global NEST J.* **2017**, *19* (2), 269−277.
(48) Balarak, D.; Joghataei, A.; Azarpira, H.; Mostafapour, F. K. Isotherms and thermodynamics of CD (II) ion removal by adsorption onto Azolla Filiculoides. *Int. J. Pharm. Technol.* **2016**, *8*, 15780−15788.
(49) Ameen Hezam Saeed, A.; Yub Harun, N.; Mahmoud Nasef, M.; Al-Fakih, A.; Abdulhakim Saeed Ghaleb, A.; Kolawole Afolabi, H. Removal of cadmium from aqueous solution by optimized rice husk biochar using response surface methodology. *Ain Shams Eng. J.* **2022**, *13* (1), 101516.
(50) Herrera, A.; Tejada-Tovar, C.; González-Delgado, Á. D. Enhancement of Cadmium Adsorption Capacities of Agricultural Residues and Industrial Fruit Byproducts by the Incorporation of Al2O3 Nanoparticles. *ACS Omega* **2020**, *5* (37), 23645−23653.
(51) Fawzy, M. A.; Darwish, H.; Alharthi, S.; Al-Zaban, M. I.; Noureldeen, A.; Hassan, S. H. A. Process optimization and modeling of Cd2+ biosorption onto the free and immobilized Turbinaria ornata using Box-Behnken experimental design. *Sci. Rep.* **2022**, *12* (1), 3256.
(52) Ayachi, F. Z.; Z Kyzas, G.; Aatrous, M.; Sakly, A.; Ben Lamine, A. Evaluating the adsorption of Ni(II) and Cu(II) on spirulina biomass by statistical physics formalism. *J. Ind. Eng. Chem.* **2019**, *80*, 461−470.
(53) Wjihi, S.; Aouaini, F.; Erto, A.; Balsamo, M.; Lamine, A. B. Advanced interpretation of CO2 adsorption thermodynamics onto porous solids by statistical physics formalism. *Chem. Eng. J.* **2021**, *406*, 126669.
(54) Khotimchenko, Y. S.; Khozhaenko, E. V.; Khotimchenko, M. Y.; Kolenchenko, E. A.; Kovalev, V. V. Carrageenans as a new source of drugs with metal binding properties. *Mar. Drugs* **2010**, *8* (4), 1106−1121.
(55) Sellaoui, L.; Dhaouadi, F.; Taamalli, S.; Louis, F.; Bakali, A. E.; Badawi, M.; Bonilla-Petriciolet, A.; Silva, L.; da Boit Martinello, K.; Dotto, G. L.; et al. Understanding the Cu2+ adsorption mechanism on activated carbon using advanced statistical physics modelling. *Environ. Sci. Pollut. Res.* **2022**, *29* (36), 54882−54889.
(56) Wjihi, S.; Erto, A.; Knani, S.; Ben Lamine, A. Investigation of adsorption process of benzene and toluene on activated carbon by means of grand canonical ensemble. *J. Mol. Liq.* **2017**, *238*, 402−410.
(57) Bouaziz, N.; Ben Manaa, M.; Aouaini, F.; Ben Lamine, A. Investigation of hydrogen adsorption on zeolites A, X and Y using statistical physics formalism. *Mater. Chem. Phys.* **2019**, *225*, 111−121.
(58) Khalfaoui, M.; Baouab, M. H. V.; Gauthier, R.; Lamine, A. B.. Statistical Physics Modelling of Dye Adsorption on Modified Cotton. *Adsorpt. Sci. Technol.* **2002**, *20* (1), 17−31.
(59) Knani, S.; Mathlouthi, M.; Ben Lamine, A. Modeling of the Psychophysical Response Curves Using the Grand Canonical Ensemble in Statistical Physics. *Food Biophys.* **2007**, *2* (4), 183−192.
(60) Diu, B.; Guthmann, C.; Lederer, D.; Roulet, B. Macroscopic motion of a totally isolated system in statistical equilibrium. *Am. J. Phys.* **1990**, *58* (10), 974−978.
(61) Khalfaoui, M.; Knani, S.; Hachicha, M. A.; Lamine, A. B. New theoretical expressions for the five adsorption type isotherms classified by BET based on statistical physics treatment. *J. Colloid Interface Sci.* **2003**, *263* (2), 350−356.
(62) Pangestuti, R.; Kim, S. K. Biological Activities of Carrageenan. In *Marine Carbohydrates: Fundamentals and Applications, Part A.*; SKBTA, K., NR, F., Eds.; Academic Press, 2014; Vol. *72*, pp 113−124..
(63) Yermak, I. M.; Barabanova, A. O.; Aminin, D. L.; Davydova, V. N.; Sokolova, E. V.; Solov'eva, T. F.; Kim, Y. H.; Shin, K. S. Effects of structural peculiarities of carrageenans on their immunomodulatory and anticoagulant activities. *Carbohydr. Polym.* **2012**, *87* (1), 713−720.
(64) Patel, S. Therapeutic importance of sulfated polysaccharides from seaweeds: updating the recent findings. *3 Biotechnol.* **2012**, *2* (3), 171−185.
(65) Gogoi, D.; Arora, N.; Kalita, B.; Sarma, R.; Islam, T.; Ghosh, S. S.; Devi, R.; Mukherjee, A. K. Anticoagulant mechanism, pharmacological activity, and assessment of preclinical safety of a novel fibrin(ogen)olytic serine protease from leaves of Leucas indica. *Sci. Rep.* **2018**, *8* (1), 6210.
(66) Bäumgen, M.; Dutschei, T.; Bornscheuer, U. T. Marine Polysaccharides: Occurrence, Enzymatic Degradation and Utilization. *ChemBioChem* **2021**, *22* (13), 2247−2256.
(67) Liang, W.; Mao, X.; Peng, X.; Tang, S. Effects of sulfate group in red seaweed polysaccharides on anticoagulant activity and cytotoxicity. *Carbohydr. Polym.* **2014**, *101*, 776−785.
(68) Karthikeyan, S.; Balasubramanian, R.; Iyer, C. S. P. Evaluation of the marine algae Ulva fasciata and Sargassum sp. for the biosorption of Cu(II) from aqueous solutions. *Bioresour. Technol.* **2007**, *98* (2), 452−455.
(69) Pavasant, P.; Apiratikul, R.; Sungkhum, V.; Suthiparinyanont, P.; Wattanachira, S.; Marhaba, T. F. Biosorption of Cu2+, Cd2+, Pb2+, and Zn2+ using dried marine green macroalga Caulerpa lentillifera. *Bioresour. Technol.* **2006**, *97* (18), 2321−2329.
(70) Sheng, P. X.; Ting, Y. P.; Chen, J. P.; Hong, L. Sorption of lead, copper, cadmium, zinc, and nickel by marine algal biomass: characterization of biosorptive capacity and investigation of mechanisms. *J. Colloid Interface Sci.* **2004**, *275* (1), 131−141.
(71) Mata, Y. N.; Blázquez, M.; Ballester, A.; González, F.; Muñoz, J. Biosorption of cadmium, lead and copper with calcium alginate xerogels and immobilized Fucus vesiculosus. *J. Hazard. Mater.* **2009**, *163* (2−3), 555−562.
(72) Romera, E.; González, F.; Ballester, A.; Blázquez, M.; Muñoz, J. Comparative study of biosorption of heavy metals using different types of algae. *Bioresour. Technol.* **2007**, *98* (17), 3344−3353.
(73) Tang, L.; Chen, Y.; Jiang, Z.; Zhong, S.; Chen, W.; Zheng, F.; Shi, G. Purification, partial characterization and bioactivity of sulfated polysaccharides from Grateloupia livida. *Int. J. Biol. Macromol.* **2017**, *94*, 642−652.
(74) Shao, P.; Chen, X.; Sun, P. Chemical characterization, antioxidant and antitumor activity of sulfated polysaccharide from Sargassum horneri. *Carbohydr. Polym.* **2014**, *105*, 260−269.
(75) Bilan, M. I.; Ustyuzhanina, N. E.; Shashkov, A. S.; Thanh, T. T. T.; Bui, M. L.; Tran, T. T. V.; Bui, V. N.; Usov, A. I. Sulfated polysaccharides of the Vietnamese brown alga Sargassum aquifolium (Fucales, Sargassaceae). *Carbohydr. Res.* **2017**, *449*, 23−31.
(76) Mao, W.; Li, H.; Li, Y.; Zhang, H.; Qi, X.; Sun, H.; Chen, Y.; Guo, S. Chemical characteristic and anticoagulant activity of the sulfated polysaccharide isolated from Monostroma latissimum (Chlorophyta). *Int. J. Biol. Macromol.* **2009**, *44* (1), 70−74.
(77) Ghanbarzadeh, M.; Golmoradizadeh, A.; Homaei, A. Carrageenans and carrageenases: versatile polysaccharides and promising marine enzymes. *Phytochem. Rev.* **2018**, *17* (3), 535−571.

https://doi.org/10.1021/acsomega.4c01540
ACS Omega 2024, 9, 23873−23891

(78) Anderson, W.; Duncan, J. G. C.; Harthill, J. E. The anticoagulant activity of carrageenan. *J. Pharm. Pharmacol.* **2011**, *17* (10), 647−654.
(79) Majumdar, S.; Chattopadhyay, P.; Mukherjee, A. K. In Vivo Anticoagulant and Thrombolytic Activities of a Fibrinolytic Serine Protease (Brevithrombolase) With the k-Carrageenan-Induced Rat Tail Thrombosis Model. *Clin. Appl. Thromb.* **2016**, *22* (6), 594−598.
(80) Jelis, E.; Kristol, D.; Arora, R. R.; Spillert, C. R.. The effect of copper ion on blood coagulation. In: *IEEE 30th Annual Northeast Bioengineering Conference, 2004. Proceedings of The*; Springfield: MA, USA.; 2004:127. doi: .
(81) Vu, T. T.; Fredenburgh, J. C.; Weitz, J. Zinc: An important cofactor in haemostasis and thrombosis. *Thromb. Haemostasis* **2013**, *109* (03), 421−430.
(82) de Araújo, C. A.; Noseda, M. D.; Cipriani, T. R.; Gonçalves, A. G.; Duarte, M. E. R.; Ducatti, D. R. B. Selective sulfation of carrageenans and the influence of sulfate regiochemistry on anticoagulant properties. *Carbohydr. Polym.* **2013**, *91* (2), 483−491.
(83) Arokiarajan, M. S.; Thirunavukkarasu, R.; Joseph, J.; Ekaterina, O.; Aruni, W. Advance research in biomedical applications on marine sulfated polysaccharide. *Int. J. Biol. Macromol.* **2022**, *194*, 870−881.
(84) Mestechkina, N. M.; Shcherbukhin, V. D. Sulfated polysaccharides and their anticoagulant activity: A review. *Appl. Biochem. Microbiol.* **2010**, *46* (3), 267−273.
(85) Nanaki, S.; Karavas, E.; Kalantzi, L.; Bikiaris, D. Miscibility study of carrageenan blends and evaluation of their effectiveness as sustained release carriers. *Carbohydr. Polym.* **2010**, *79* (4), 1157−1167.

https://doi.org/10.1021/acsomega.4c01540
ACS Omega 2024, 9, 23873−23891